2022-12

EXPERIMENTAL ASSESSMENT OF A NOVEL DUAL OPENING DEWAR FOR USE ON A LIQUID AIR ENERGY STORAGE SYSTEM INSTALLED ON REMOTE, ISLANDED, RENEWABLE MILITARY MICROGRIDS

Fackrell, Christofer J.

Monterey, CA; Naval Postgraduate School

NAVAL POSTGRADUATE SCHOOL

MONTEREY, CALIFORNIA

THESIS

EXPERIMENTAL ASSESSMENT OF A NOVEL DUAL OPENING DEWAR FOR USE ON A LIQUID AIR ENERGY STORAGE SYSTEM INSTALLED ON REMOTE, ISLANDED, RENEWABLE MILITARY MICROGRIDS

by

Christofer J. Fackrell

December 2022

Thesis Advisor: Anthony G. Pollman
Co-Advisors: Anthony J. Gannon
Douglas L. Van Bossuyt

THIS PAGE INTENTIONALLY LEFT BLANK

REPORT DOCUMENTATION PAGE	*Form Approved OMB No. 0704-0188*

1. AGENCY USE ONLY *(Leave blank)*	**2. REPORT DATE** December 2022	**3. REPORT TYPE AND DATES COVERED** Master's thesis

4. TITLE AND SUBTITLE
EXPERIMENTAL ASSESSMENT OF A NOVEL DUAL OPENING DEWAR FOR USE ON A LIQUID AIR ENERGY STORAGE SYSTEM INSTALLED ON REMOTE, ISLANDED, RENEWABLE MILITARY MICROGRIDS

5. FUNDING NUMBERS

6. AUTHOR(S) Christofer J. Fackrell

7. PERFORMING ORGANIZATION NAME(S) AND ADDRESS(ES)
Naval Postgraduate School
Monterey, CA 93943-5000

8. PERFORMING ORGANIZATION REPORT NUMBER

9. SPONSORING / MONITORING AGENCY NAME(S) AND ADDRESS(ES)
N/A

10. SPONSORING / MONITORING AGENCY REPORT NUMBER

11. SUPPLEMENTARY NOTES The views expressed in this thesis are those of the author and do not reflect the official policy or position of the Department of Defense or the U.S. Government.

12a. DISTRIBUTION / AVAILABILITY STATEMENT
Approved for public release. Distribution is unlimited.

12b. DISTRIBUTION CODE
A

13. ABSTRACT (maximum 200 words)

Islanded, renewable energy microgrids for use at remote Department of Defense (DOD) facilities reduce logistical burdens associated with fossil fuel–based electrical power sources and provide greater operational flexibility; however, energy generation can be intrinsically intermittent on these microgrids. This intermittent electrical generation can be mitigated with energy storage. Liquid air energy storage (LAES) is one promising technology proposed to meet this energy storage issue due to its high energy density. Small-scale microgrids may not have enough excess capacity to store pressurized liquid air (LA), and instead may rely on unpressurized LA storage and their associated unpressurized power recovery options. Using commercial off-the-shelf components, this thesis conducts a comparative tradespace study for a variety of dual opening, unpressurized Dewar designs for use with Stirling- or Peltier-based power recovery cycles. The dual opening design is found to not be efficacious for short-term storage necessary for microgrid use due to excessive conductive losses to the outer Dewar shell; however, the design may be useful as an LA receiver and immediate-use energy storage medium for a connected Stirling generator. A proposed alternative solution using Dewar self-pressurization for LA storage and transport for DOD microgrid applications is presented for future work.

14. SUBJECT TERMS Dewar, liquid air, LA, liquid air energy storage, LAES, renewable microgrid, islanded microgrid, remote microgrid, Stirling generator, Stirling cryocooler, Peltier thermoelectric generator	**15. NUMBER OF PAGES** 71
	16. PRICE CODE

17. SECURITY CLASSIFICATION OF REPORT	**18. SECURITY CLASSIFICATION OF THIS PAGE**	**19. SECURITY CLASSIFICATION OF ABSTRACT**	**20. LIMITATION OF ABSTRACT**
Unclassified	Unclassified	Unclassified	UU

NSN 7540-01-280-5500

Standard Form 298 (Rev. 2-89)
Prescribed by ANSI Std. 239-18

THIS PAGE INTENTIONALLY LEFT BLANK

Approved for public release. Distribution is unlimited.

EXPERIMENTAL ASSESSMENT OF A NOVEL DUAL OPENING DEWAR FOR USE ON A LIQUID AIR ENERGY STORAGE SYSTEM INSTALLED ON REMOTE, ISLANDED, RENEWABLE MILITARY MICROGRIDS

Christofer J. Fackrell
Lieutenant Commander, United States Navy
BS, Oregon State University, 2011
MEM, Old Dominion University, 2018

Submitted in partial fulfillment of the
requirements for the degree of

MASTER OF SCIENCE IN SYSTEMS ENGINEERING

from the

NAVAL POSTGRADUATE SCHOOL
December 2022

Approved by: Anthony G. Pollman
Advisor

Anthony J. Gannon
Co-Advisor

Douglas L. Van Bossuyt
Co-Advisor

Oleg A. Yakimenko
Chair, Department of Systems Engineering

THIS PAGE INTENTIONALLY LEFT BLANK

ABSTRACT

Islanded, renewable energy microgrids for use at remote Department of Defense (DOD) facilities reduce logistical burdens associated with fossil fuel–based electrical power sources and provide greater operational flexibility; however, energy generation can be intrinsically intermittent on these microgrids. This intermittent electrical generation can be mitigated with energy storage. Liquid air energy storage (LAES) is one promising technology proposed to meet this energy storage issue due to its high energy density. Small-scale microgrids may not have enough excess capacity to store pressurized liquid air (LA), and instead may rely on unpressurized LA storage and their associated unpressurized power recovery options. Using commercial off-the-shelf components, this thesis conducts a comparative tradespace study for a variety of dual opening, unpressurized Dewar designs for use with Stirling- or Peltier-based power recovery cycles. The dual opening design is found to not be efficacious for short-term storage necessary for microgrid use due to excessive conductive losses to the outer Dewar shell; however, the design may be useful as an LA receiver and immediate-use energy storage medium for a connected Stirling generator. A proposed alternative solution using Dewar self-pressurization for LA storage and transport for DOD microgrid applications is presented for future work.

THIS PAGE INTENTIONALLY LEFT BLANK

TABLE OF CONTENTS

THIS PAGE INTENTIONALLY LEFT BLANK

LIST OF FIGURES

THIS PAGE INTENTIONALLY LEFT BLANK

LIST OF TABLES

THIS PAGE INTENTIONALLY LEFT BLANK

LIST OF ACRONYMS AND ABBREVIATIONS

CAES	Compressed Air Energy Storage
COTS	Commercial Off-the-Shelf
DOD	Department of Defense
DOE	Department of Energy
EDG	Emergency Diesel Generator
EPP	Electronic Power Processor
LA	Liquid Air
LAES	Liquid Air Energy Storage
LN2	Liquid Nitrogen
PCC	Point of Common Coupling
PLA	Polylactic Acid
SD	Standard Deviation
TEG	Thermoelectric Generator
U.S.C.	United States Code

THIS PAGE INTENTIONALLY LEFT BLANK

EXECUTIVE SUMMARY

The Department of Defense (DOD) is interested in energy storage options for use on remote, islanded, and renewable energy microgrids which power remote and forward deployed military installations [1]. This interest stems from the logistical burdens and constraints associated with the typical source of electrical power for these types of facilities detached from regional power grids, which are typically diesel generators [2]. While diesel generators can supply a large amount of electrical power, they rely on a steady source of fuel. Renewable energy-based microgrids have the potential to bypass this logistical burden but must overcome the intrinsically intermittent power production associated with renewable energy, as well as the storage of energy for use when the renewable energy source is limited (e.g., at night when using photovoltaic cells) [3].

Liquid air energy storage (LAES) is an attractive option for storing excess energy on a renewable microgrid due to its high energy density and lack of geographical constraints, being producible if there is sufficient excess energy on the microgrid [4]. Previous investigations in this area by Bailey et al. have resulted in the development of a Stirling-Stirling liquid air (LA) battery using a Stirling cryocooler to produce LA and a Stirling generator for electrical power recovery from the medium [5]. To enable this configuration, a wide mouth Dewar is used to directly incorporate the Stirling generator by introducing the LA from the top of the Dewar, a design that can dramatically increase thermal losses at the neck of the Dewar.

This thesis explores the use of a dual opening Dewar to address the thermal limitations of Bailey et al.'s design. This design has a narrower upper Dewar neck and a fitting at the bottom of the Dewar to provide temperature differential to a Stirling generator across the fitting, or for LA transport to a thermoelectric generator (TEG). This investigation found that for a small volume (473 ml) Dewar, the dual neck design was 12.1% as efficient as an unmodified Dewar with no bottom neck. This efficiency does not meet the short-term (i.e., 24 hours) LA storage requirements for a microgrid using a LAES system; however, as a receiving vessel for LA that will be immediately used for energy recovery, the duel neck design works well, as the energy losses at the bottom

Dewar neck could be directly used for electrical power recovery via a Stirling generator or TEG, or a combination of these two methods.

The work presented also illustrates the importance of a vacuum jacket in any Dewar design, as well as the advantageous thermal properties of Teflon components used in cryogenic applications due to their low thermal conductivity. It is recommended that future work explores the use of a low-pressure, self-pressurizing Dewar design that takes advantage of commercial-off-the-shelf (COTS) components leveraging minimal modification. A self-pressurizing design is proposed in this work and would allow for the power recovery component of a LAES system to be physically separated from the stored LA until needed for use, providing an increase in efficiency over the patented designs by both Bailey et al. and the novel Dewar design presented in this research.

References

[1] D. T. Ton and M. A. Smith, "The U.S. Department of Energy's microgrid initiative," *Electr. J.*, vol. 25, no. 8, pp. 84–94, Oct. 2012 [Online]. Available: https://doi.org/10.1016/j.tej.2012.09.013.

[2] R. Haerer, "Whack-a-mole fuel selection: Reducing operational risks and mitigating new challenges in the U.S. Department of Defense." Climate and Security Fellowship Program, Oct. 2021. [Online]. Available: https://climateandsecurity.org/wp-content/uploads/2021/10/Climate-Security-Risk-Briefers_Climate-and-Security-Fellows-Program_October-2021-1.pdf#page=27

[3] A. Kafetzis, C. Ziogou, K. D. Panopoulos, S. Papadopoulou, P. Seferlis, and S. Voutetakis, "Energy management strategies based on hybrid automata for islanded microgrids with renewable sources, batteries and hydrogen," *Renew. Sustain. Energy Rev.*, vol. 134, p. 110118, Dec. 2020 [Online]. Available: https://doi.org/10.1016/j.rser.2020.110118.

[4] S. X. Wang, X. D. Xue, X. L. Zhang, J. Guo, Y. Zhou, and J. J. Wang, "The application of cryogens in liquid fluid energy storage systems," *Phys. Procedia*, vol. 67, pp. 728–732, Jan. 2015 [Online]. Available: https://doi.org/10.1016/j.phpro.2015.06.123.

[5] N. A. Bailey, C. M. Girouard, and A. G. Pollman, "Dual Stirling cycle liquid air battery," US20220042478A1, Feb. 10, 2022 Accessed: Aug. 03, 2022. [Online]. Available: https://patents.google.com/patent/US20220042478A1/en

ACKNOWLEDGMENTS

I sincerely thank my thesis advisors, Dr. Anthony Pollman, Dr. Douglas Van Bossuyt, and Dr. Anthony Gannon, for their professionalism, mentorship, and guidance. You helped me improve as a technical writer and scholar.

To my wife, Rebecca, thank you for being there for me every step of the way on this academic journey. You helped me focus on my work, but also reminded me there is more to life than work. To my children, Wesley and Elizabeth, thank you for understanding that I didn't always have the time to spend with you that I would have liked to have.

THIS PAGE INTENTIONALLY LEFT BLANK

I. INTRODUCTION

Historically, electrical grid energy sources have primarily come from fossil fuel based regional power stations, with backup sources of electrical power at the Department of Defense (DOD) installation or facility level most commonly taking the form of emergency diesel generators (EDGs) [1], [2]. Conventionally, this approach has provided low-cost, energy dense emergency power to critical loads when normal utility power is lost; however, these EDGs are generally operated individually and do not connect intelligently with each other or the power grid to which they are connected [3]. This lack of intelligent interconnectedness increases the vulnerability of the system to electrical supply interrupts, which in turn lowers efficiency, productivity, and mission readiness [4]. Over the last several years there has been an increased interest by the DOD regarding remote, islanded, and renewable energy microgrids for use in remote locations to address these efficiency and productivity issues, as well as allowing for a reduction in logistics burdens associated with fossil fuel based electrical power sources [2], [5].

The Department of Energy (DOE) defines a microgrid as "a group of interconnected loads and distributed energy resources within clearly defined electrical boundaries that acts as a single controllable entity with respect to the [electrical] grid. A microgrid can connect and disconnect from the grid to enable it to operate in both grid-connected or islanded-mode" [6, p. 84]. This definition can be modified to define a remote, islanded microgrid as one that does not connect to a larger, regional power grid [7]. Furthermore, a remote, islanded, and renewable microgrid is one that supplies the majority of its electrical power from renewable sources, such as wind and solar [3].

Hirsch et al. expand on the DOE's definition of a microgrid and describe three core requirements a microgrid must possess; these requirements are that it is identifiable, independent, and intelligent [8], [9]. To satisfy being identifiable, the microgrid must have clearly defined physical and functional boundaries, which are defined by those components, software, and functional elements which provide an external interface between the microgrid and the external utility power grid, also called a point of common coupling (PCC) [1], [10]. Additionally, the identifiable boundary encompasses those

personnel working for organizations in charge of maintaining, operating, or administrating these systems [9], [11]. The requirement of being independent refers to the ability of the microgrid to provide sufficient electrical power to end-user sites when disconnected from a utility power grid, typically using multiple redundant power sources [6], [12]. Common power sources include natural gas, biogas, solar, wind, fuel-cells, diesel generators, or micro-turbines [1]. Finally, a microgrid fulfills the requirement of being intelligent through the use of a controller, the defining technology that enables the microgrid to manage energy generation, storage, and electrical loads within the microgrid boundaries [13], [14]. These controllers are also called electronic power processors (EPPs) and allow communication between microgrid components, enabling either centralized or distributed control over both active and reactive control of microgrid functions; these functions serve to maximize power availability to loads within the microgrid boundary [15]. The benefits of using microgrids are not limited to minimizing power loss to electrical loads. Microgrids can improve efficiency, lower energy consumption, reduce cost, limit environmental impact through use of renewables, and improve energy reliability and resilience when compared to traditional utility power grids [16]. Of these benefits, the DOD focuses on efficiency, reliability, and resilience, which collectively is referred to as energy security [17]. Per United States Code (U.S.C.) 10, this focus on energy security is to maximize mission readiness for all United States armed services.

While the use of remote, islanded, renewable microgrids aim to address electrical energy supply issues for remote DOD facilities, the energy generated by them is intrinsically intermittent due to the microgrid's reliance on renewable energy sources [18]. This can be mitigated with energy storage [19]. Energy storage on microgrids during power interruption presents its own problems [20]. Typically, when renewable energy supply is greater than demand the supply is metered down as in the case of wind turbines, or it is rejected as heat via a resister bank for non-adjustable sources such as solar; however, with attached microgrid energy storage this excess electrical power can be used to store energy for later use [21], [22]. Several generalized types of energy storage systems exist including electrical, mechanical, thermal, chemical,

electrochemical, and magnetic; each of these solutions has their own set of advantages and disadvantages, including cost, size, energy density, efficiency, lifespan, charging rate, reliability, ease of use, environmental impact, life cycle cost, and disposability [1], [23], [24]. Additionally, depending on the storage method, the energy recovery options are limited, with each option having its own advantages and disadvantages [25]. This work focuses on thermal energy storage in the form of cryogenic liquid air (LA).

Typically, liquid air energy storage (LAES) systems are used for large or industrial-scale applications due to inefficiencies in liquifying air which use certain thermo-dynamic cycles, such as the Linde Hampson, Claude, mixed refrigerant, and Solvay cycles [26]–[28]. However, at smaller-scales, which would be viable on a islanded microgrid, these liquefaction and power-recovery cycles are inappropriate due to electrical requirements for LA production or the size of the components in a traditional LAES system, thus other processes are considered. This consideration at the microgrid level is made due to its high energy density of LA and lack of geographic requirements like many similar renewable energy capture and storage techniques, such as compressed air energy storage (CAES) and pumped hydro [29], [30]. The most common low-power liquefaction options include the Stirling, pulse tube, Gifford-McMahon, Brayton, and Joule-Thomson cycles [28]. This combination of unfettered access to air, coupled with a high energy density, makes investigation into LAES for remote, islanded, renewable microgrids a useful endeavor.

Previous work on small-scale LAES has mainly focused on feasibility, modeling, or component performance analyses. Building on the work of Joshi and Patel, and Howe et al., Willis et al. modeled a small-scale liquid air energy storage and expansion system using a process modeling and simulation software common to the oil and gas industry [31]–[33]. Girouard et al. and Fredrickson et al. proposed component selection for a scaled-down version of an industrial LA energy storage process [34], [35]. However, these investigations showed that turbine and other similar technologies do not scale well, and subsequent analyses focused on cycles and technologies that were more promising for small-scale applications, agreeing with work presented by

Damak et al. [27], [36]–[39]. Two of these promising small-scale energy recovery methods are a Stirling generator, using a Stirling cycle, and a thermoelectric generator, leveraging the Peltier effect [38], [40].The patent application for a dual Stirling cycle liquid air battery by Bailey et al. uses a wide mouth Dewar that contains both a Stirling cryocooler for liquefaction and Stirling generator power recovery [38].

A Dewar is a vessel designed to store cryogenic fluids by minimizing heating of the stored fluid by conduction, convection, and radiative heat transfer [41]. In its simplest form, a Dewar has an inner and outer wall with a vacuum drawn between them to minimize thermal conductivity, a low emissivity reflective radiation shield to minimize radiative heating, and a lid or stopper to minimize the vapor mass flow of the stored liquid as it evaporates, thus limiting thermal convection [42]. Atmospherically vented storage Dewars typically use a longer and narrow neck, as this lows the overall heat flux conducted down the neck, reducing evaporation rate [43], [44]. Additionally, typical storage Dewars contain a spherical or semi-spherical storage area to maximize the volume of LA to the surface area of the Dewar's material in contact with the LA [44]. This reduces conductive losses of the LA. The wide mouth Dewar design used by Bailey et al., necessary to support a Stirling cryocooler and generator in one opening, increases the possibility of losses to convection compared to narrow neck variants, and relies on an extended cold side of the Stirling generator to be in contact with LA throughout the storage volume, which also increases conduction [38].

This thesis explores alternatives to Bailey et al.'s Dewar design that may be efficacious in improving energy extraction from liquid air in small-scale applications using a non-pressurized LA storage and energy recovery system, as well as expand the compatible types of energy storage associated with the Dewar. Specifically, it explores the use of a two opening Dewar, with the opening at the top designated for a cryocooler to produce LA and a second penetration of the Dewar at the bottom used for a power recovery cycle. This design reduces the width of the upper Dewar neck, reducing convection from the surface of the LA while also reducing the higher conductivity associated with a wider Dewar mouth. The lower port allows for energy extraction from the LA's entire stored volume as it evaporates without the need for an extended cold side

for an attached Stirling generator. This configuration does increase the conductive losses of the Dewar, which is the tradespace that will be explored. Additionally, this Dewar configuration could be adapted to other low pressure energy recovery methods, such as a thermoelectric generator.

This thesis uses the ``manuscript option'' as defined in [45]. The structure of the thesis is: Chapter 1 provides DOD-focused context of the research; Chapter 2 presents the journal manuscript that was submitted to Multidisciplinary Digital Publishing Institute's (MDPI's) *Inventions* journal for peer review; Chapter 3 provides the physical experimental setup and experimental data collected; Chapter 4 presents the preliminary patent Dewar design that was submitted as a result of this thesis; and Chapter 5 summarizes the findings of the research in a DOD context, an expands upon future research specifically of interest to the defense community.

THIS PAGE INTENTIONALLY LEFT BLANK

II. MANUSCRIPT SUBMISSION

A. EXPERIMENTAL ASSESSMENT OF A NOVEL DUAL OPENING DEWAR FOR USE ON A LIQUID AIR ENERGY STORAGE SYSTEM INSTALLED ON REMOTE, ISLANDED, RENEWABLE MILITARY MICROGRIDS

A version of this chapter was submitted to the MDPI *Inventions* journal on September 22, 2022, as: Christofer Fackrell, Anthony Pollman, Douglas L. Van Bossuyt, and Anthony J. Gannon, "Experimental Assessment of a Novel Dual Opening Dewar for Use on a Liquid Air Energy Storage System Installed on Remote, Islanded, Renewable Microgrids."

B. INTRODUCTION

Historically, electrical grid energy sources have primarily come from fossil fuel based regional power stations, with backup sources of electrical power at an installation or facility level most commonly taking the form of emergency diesel generators (EDGs) [1]. This energy distribution model does not work when a regional power grid is unavailable. Over the last several years there has been an increased interest regarding remote, islanded, and renewable energy microgrids for use in remote locations, allowing for a reduction in logistics burdens associated with fossil fuel based electrical power sources [2], [5]. The Department of Energy (DOE) defines a microgrid as "a group of interconnected loads and distributed energy resources within clearly defined electrical boundaries that acts as a single controllable entity with respect to the [electrical] grid. A microgrid can connect and disconnect from the grid to enable it to operate in both grid-connected or islanded-mode" [6](p. 84). This definition can be extended to define a remote islanded microgrid as one that does not connect to a larger, regional power grid [7]. Furthermore, a remote, islanded, and renewable microgrid is one that supplies

the majority of its electrical power from renewable sources, such as wind and solar [3]. While these remote, islanded, renewable microgrids aim to address electrical energy supply issues for isolated locations, the energy generated by them is intrinsically intermittent due to the microgrid's reliance on renewable energy sources [18]. This can be mitigated with energy storage [19].

Energy storage on microgrids during power interruption presents its own problems [20]. Typically, when renewable energy supply is greater than demand the supply is metered down as in the case of wind turbines, or it is rejected as heat via a resister bank for non-adjustable sources such as solar; however, with attached microgrid energy storage this excess electrical power can be used to store energy for later use [21], [22]. Several generalized types of energy storage systems exist including electrical, mechanical, thermal, chemical, electrochemical, and magnetic; each of these solutions has their own set of advantages and disadvantages, including cost, size, energy density, efficiency, lifespan, charging rate, reliability, ease of use, environmental impact, life cycle cost, and disposability [1], [23], [24]. Additionally, depending on the storage method, the energy recovery options are limited, with each option having its own advantages and disadvantages [25]. This work focuses on thermal energy storage in the form of cryogenic liquid air (LA).

Typically, liquid air energy storage (LAES) systems are used for large or industrial-scale applications due to inefficiencies in liquifying air which use certain thermo-dynamic cycles, such as the Linde Hampson, Claude, mixed refrigerant, and Solvay cycles [26]–[28]. However, at smaller-scales, which would be viable on a islanded microgrid, these liquefaction and power-recovery cycles are inappropriate due to electrical requirements for LA production or the size of the components in a traditional LAES system, thus other processes are considered. This consideration at the microgrid level is made due to its high energy density of LA and lack of geographic requirements like many similar renewable energy capture and storage techniques, such as compressed air energy storage (CAES) and pumped hydro [29], [30]. The most common low-power liquefaction options include the Stirling, pulse tube, Gifford-McMahon, Brayton, and Joule-Thomson cycles [28]. This combination of unfettered access to air, coupled with a

high energy density, makes investigation into LAES for remote, islanded, renewable microgrids a useful endeavor.

Previous work on small-scale LAES has mainly focused on feasibility, modeling, or component performance analyses. Building on the work of Joshi and Patel, and Howe et al., Willis et al. modeled a small-scale liquid air energy storage and expansion system using a process modeling and simulation software common to the oil and gas industry [31]–[33]. Girouard et al. and Fredrickson et al. proposed component selection for a scaled-down version of an industrial LA energy storage process [34], [35]. However, these investigations showed that turbine and other similar technologies do not scale well, and subsequent analyses focused on cycles and technologies that were more promising for small-scale applications, agreeing with work presented by Damak et al. [27], [36]–[39]. Two of these promising small-scale energy recovery methods are a Stirling generator, using a Stirling cycle, and a thermoelectric generator, leveraging the Peltier effect [38], [40].The patent application for a dual Stirling cycle liquid air battery by Bailey et al. uses a wide mouth Dewar that contains both a Stirling cryocooler for liquefaction and Stirling generator power recovery [38].

A Dewar is a vessel designed to store cryogenic fluids by minimizing heating of the stored fluid by conduction, convection, and radiative heat transfer [41]. In its simplest form, a Dewar has an inner and outer wall with a vacuum drawn between them to minimize thermal conductivity, a low emissivity reflective radiation shield to minimize radiative heating, and a lid or stopper to minimize the vapor mass flow of the stored liquid as it evaporates, thus limiting thermal convection [42]. Atmospherically vented storage Dewars typically use a longer and narrow neck, as this lows the overall heat flux conducted down the neck, reducing evaporation rate [43], [44]. Additionally, typical storage Dewars contain a spherical or semi-spherical storage area to maximize the volume of LA to the surface area of the Dewar's material in contact with the LA [44]. This reduces conductive losses of the LA. The wide mouth Dewar design used by Bailey et al., necessary to support a Stirling cryocooler and generator in one opening, increases the possibility of losses to convection compared to narrow neck variants, and relies on an

extended cold side of the Stirling generator to be in contact with LA throughout the storage volume, which also increases conduction [38].

This thesis explores alternatives to Bailey et al.'s Dewar design that may be efficacious in improving energy extraction from liquid air in small-scale applications using a non-pressurized LA storage and energy recovery system, as well as expand the compatible types of energy storage associated with the Dewar. Specifically, it explores the use of a two opening Dewar, with the opening at the top designated for a cryocooler to produce LA and a second penetration of the Dewar at the bottom used for a power recovery cycle. This design reduces the width of the upper Dewar neck, reducing convection from the surface of the LA while also reducing the higher conductivity associated with a wider Dewar mouth. The lower port allows for energy extraction from the LA's entire stored volume as it evaporates without the need for an extended cold side for an attached Stirling generator. This configuration does increase the conductive losses of the Dewar, which is the tradespace that will be explored. Additionally, this Dewar configuration could be adapted to other low pressure energy recovery methods, such as a thermoelectric generator.

C. MATERIALS AND METHODS

This research utilized commercial off-the-shelf (COTS) components and readily available additive manufactured apparatuses to explore the tradespace of a dual opening Dewar. This comparison was done by measuring the evaporation rate (g/min) of liquid nitrogen (LN2), which is readily commercially available, for each Dewar configuration and graphing the result.

To facilitate rapid, low-cost Dewar experimentation, 473 ml Hydro Flask TempShield bottles were used, which were found to have a comparable physical design to typical experimental Dewars and have been shown to be efficacious in in approximating their performance [42], [46]. These bottles contain a 1mm thick stainless-steel outer shell, a 0.75 mm thick stainless-steel inner shell, a vacuum jacket between these shells, and physical contact between the shells only occurring at the top mouth of

the bottle. The baseline bottle was modified to create an additional five experimental Dewar configurations.

Each flask was placed on a 3D printed polylactic acid (PLA) plastic cylinder (3 in outside diameter, 2 in inside diameter, 2 in height, density 0.33 g/cm^3). The 2 in inner cavity of the plastic cylinder was filled with low-density polyurethan ether foam (density 0.03 g/cm^3) to provide support for experimental Dewar modifications. An additional polyurethan ether foam cylinder (62 mm diameter, 50 mm height) was used to cover the mouth of the experimental Dewars to limit convective heat transfer.

Data collection runs started with a temperature equalization step, which required filling the experimental Dewar with 350 g of LN2 and allowing 300 g of LN2 to evaporate, or 1 hour to elapse. After temperature equalization, the experimental Dewar was once again filled to a level of 350 g of LN2 and evaporation data was recorded and graphed between LN2 levels of 300 g to the first LN2 mass measurement of 50 g, or less, on its standard data recording cycle. Mass data was recorded once per minute for the modified experimental Dewars and once per 10 minutes for the baseline, unmodified experimental configuration. To measure the change in LN2 mass, two laboratory scales were used: an Ohaus CS 5000 and a Bonvoisin BCS-30. Four data runs for each experimental configuration were conducted and then averaged together. The experimental results were graphed and normalized exponential decay evaporation equations were determined using MATLAB which approximated the various complex heat transfer mechanism taking place [41]. Stagnant air within the experimental area was maintained to the greatest extent possible to limit airflow and changes in humidity, ambient temperature ranged from 20.1 C to 21.9 C, and lighting conditions were maintained constant. The basic experimental setup is shown in Figure 1.

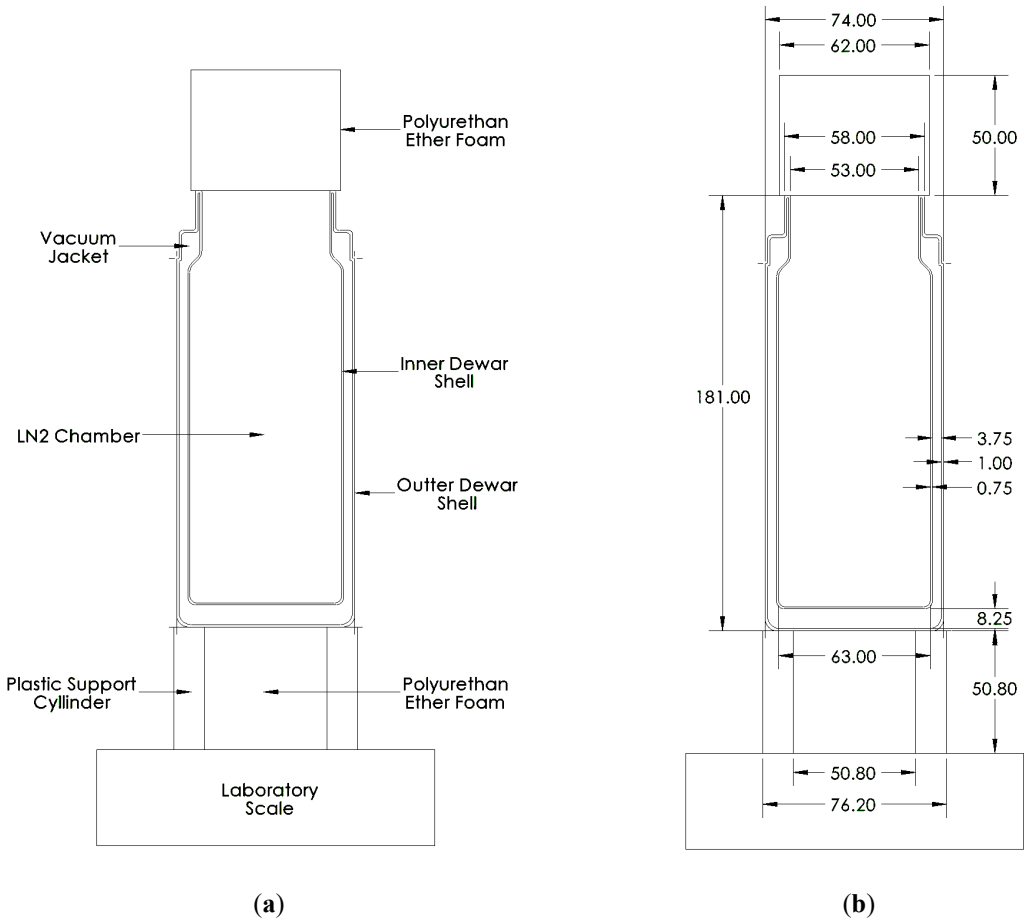

(a) Basic experimental setup with component labels with baseline configuration shown; (**b**) Basic experimental setup characteristic dimensions with baseline configuration shown. All measurements are shown in mm.

Figure 1. Basic Experimental Setup

Six different experimental Dewar configurations were analyzed for LN2 evaporation rates: a baseline, unmodified 473 ml Hydro Flask TempShield bottle; an experimental Dewar configuration that modifies the baseline by removing the vacuum jacket; an experimental Dewar configuration without a vacuum jacket containing a brass fitting at the bottom of the Dewar that does not come in physical contact with the outer Dewar shell; an experimental Dewar configuration without a vacuum jacket with a Teflon fitting at the bottom of the Dewar; an experimental Dewar configuration without a vacuum jacket and a brass fitting at the bottom of the Dewar; and an experimental Dewar with a vacuum jacket and a brass fitting at the bottom of the Dewar. The baseline Dewar

configuration did not modify the physical structure of the bottle, while five of the experimental Dewar configurations modified this baseline in some way.

The experimental Dewar without a vacuum jacket modified the baseline configuration by drilling a 5/32 in (4 mm) hole into the center-bottom of the baseline bottle's outer shell. The purpose of this test configuration was to measure the effect of the vacuum jacket on LN2 evaporation rate compared to the baseline.

The experimental Dewar without a vacuum jacket with a brass fitting at the bottom of the Dewar that does not come in physical contact with the outer Dewar shell was modified to assess the effect of conduction between the brass fitting and the outer Dewar shell. A 1–9/64 in (29 mm) hole was drilled in the center-bottom of the outer Dewar shell and a 1/4 in NPT threaded tap was drilled into the center-bottom of the inner shell. A 1/4 in NPT, 1–1/2 in long, brass double end threaded fitting with a 1/4 in NPT cap on one side was then threaded into the tap on the inner Dewar wall and sealed with cryogenic rated Scotch-Weld Epoxy Adhesive 2216 B/A Gray.

The experimental Dewar with a vacuum jacket and a brass fitting at the bottom of the Dewar was modified to support the bottom brass fitting and to restore the vacuum to the Dewar. A 1/4 in NPT threaded tap was drilled into the center-bottom of the Dewar's inner and outer shell. A 1/4 in NPT, 1–1/2 in long, brass dual threaded fitting with a 1/4 in NPT cap was then threaded into this tap and sealed with cryogenic rated Scotch-Weld Epoxy Adhesive 2216 B/A Gray. A 1/4in NPT hole was also drilled into the outer Dewar wall 90mm from the base. This allowed for a 1/4 in NPT brass vacuum ball valve to be installed with a 1/4 in brass barbed hose fitting, permitting a 29.9 in Hg vacuum to be drawn between the inner and outer Dewar shells; the Scotch-Weld Epoxy Adhesive 2216 B/A Gray was used to seal the vacuum ball valve to the outer Dewar wall. This configuration allowed for assessment of the effect conduction through the brass fitting to the outer Dewar wall had on LN2 evaporation rate. This same experimental Dewar configuration was also used to determine the LN2 evaporation rate without a vacuum by opening the brass vacuum ball valve.

The experimental Dewar without a vacuum jacket and a Teflon fitting at the bottom of the Dewar was modified in the same way as the Dewar with a vacuum jacket and a brass fitting, except a Teflon fitting of the same dimensions as the brass fitting was used; however, a constant vacuum could not be maintained using the Teflon fitting. This configuration enabled assessing the use of a Teflon, vice brass, fitting material. This was done because Teflon has a lower heat transfer coefficient than brass, which was hypothesized to lower convective heat losses compared to an equivalent experiment using brass [47].

These six experimental configurations were assigned an experiment configuration designator per Table 1.

Table 1. Experimental Dewar Configuration Designations

Experimental Dewar Configuration	Description
A	Baseline 473 ml Hydro Flask TempShield bottle-Dewar with no modification. Contains a vacuum jacket.
B	Modified baseline bottle-Dewar with a hole in the bottom outer shell and no vacuum jacket.
C	Modified baseline bottle-Dewar with a hole in the bottom outer and inner shells, a bottom mounted capped brass fitting that does not have metal-metal conduction to the outer bottle-Dewar shell, and no vacuum jacket.
D	Modified baseline bottle-Dewar with a capped threaded Teflon fastener penetrating the bottom outer and inner shells with no vacuum jacket.
E	Modified baseline bottle-Dewar with a capped threaded brass fastener penetrating the bottom outer and inner shells with no vacuum jacket.
F	Modified baseline bottle-Dewar with a capped threaded brass fastener penetrating the bottom outer and inner shells with a vacuum jacket.

Experimental Dewar configuration designations for the baseline Hydro Flask and five modified configurations of the baseline.

Physical representations of the experimental Dewar configurations are shown in Figure 2. The scale, PLA support cylinder, and low-density polyurethan ether foam are not shown but are the same as in Figure 1. Specific Dewar measurements are not shown but are to scale to those provided in Figure 1.

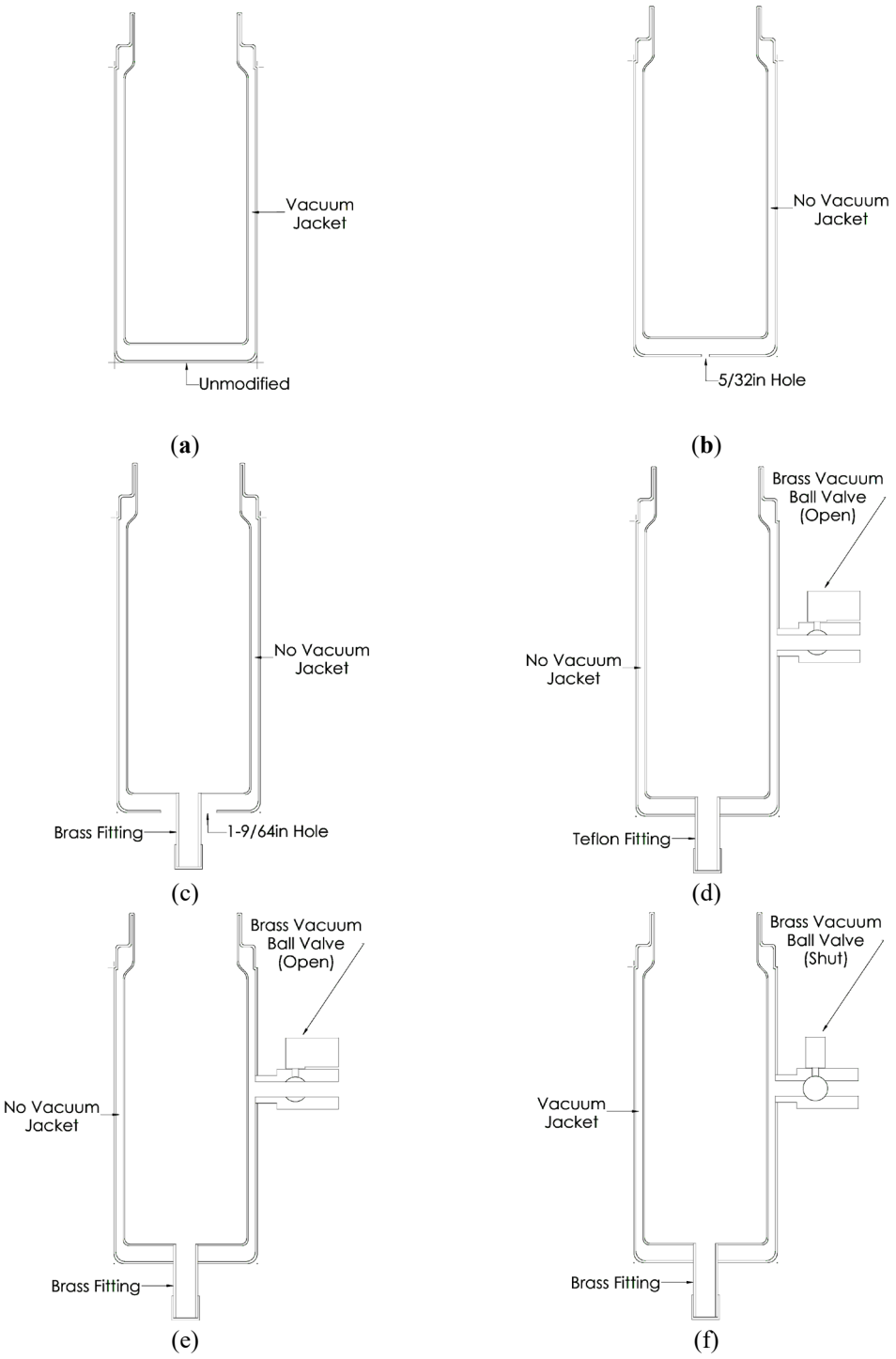

(a) Experimental configuration A; (b) Experimental configuration B; (c) Experimental configuration C; (d) Experimental configuration D; (e) Experimental configuration E; (f) Experimental configuration F. A 1/4 in brass barbed hose fitting was attached to the vacuum ball value for experimental configurations D, E, and F, but are not shown in this figure.

Figure 2. Experimental Configurations

D. RESULTS

Each experimental Dewar had four data runs collected. The average results of these runs for configurations B through F are shown in Figure 3.

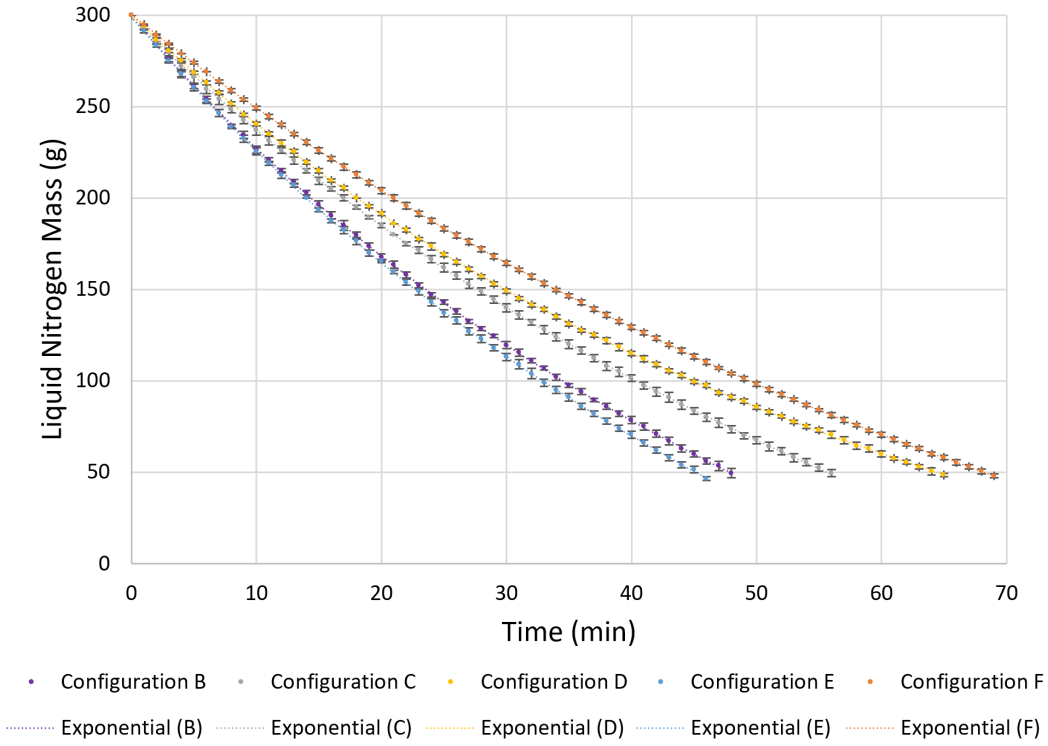

Each curve is the average of four data runs, with data plotted in one-minute increments. Each data point contains y-axis LN2 mass error bars. All curves start at 300 g of LN2 and continue until the first averaged data point is less than or equal to 50 g of LN2.

Figure 3. Evaporation Rates for Dewar Configurations B, C, D, E, and F

The performance of each experimental Dewar is based on the Dewar's rate of LN2 evaporation, with higher evaporation rates being considered worse performance and lower evaporation rates being considered better. Experimental Dewar configuration F had the lowest evaporation rate among the modified Dewars, evaporating from 300 g of LN2 to 48 g of LN2 in 69 minutes. Aside from the baseline experimental Dewar configuration A, presented in Figure 4 which evaporates from 300 g to 49g of LN2 in 570 minutes, configuration F was the only Dewar configuration which contained a vacuum jacket, highlighting the importance of a vacuum jacket with regards to Dewar performance.

Despite this performance, the holding time of LN2 for Dewar configuration F is only 12.1% of Dewar configuration A. This is due to conduction directly to the outer Dewar shell via the brass fitting.

The worst performing experimental Dewar was configuration E, which had 253.5 g of LN2 evaporation in 46 minutes. The difference between this configuration and configuration F was that the vacuum port for configuration E was opened to remove the vacuum jacket. The removal of the vacuum allowed air to be in the vacuum space, dramatically increasing the convection taking place between the inner Dewar shell to the outer Dewar shell. Additionally, gaseous airflow can occur at the opening of the vacuum ball valve, meaning an increase in convective heat transfer occurs as warm air is permitted to more freely flow into the gap between the Dewar shells. This performance drop between the best and worst performing configurations once again emphasizes the importance of a vacuum jacket between Dewar shells to reduce thermal convective and conductive losses.

The second best performing experimental Dewar was configuration D, which had 251.5 g of LN2 evaporating in 65 minutes. Two differences existed between this configuration and configuration F. First, no vacuum jacket existed, with air being permitted to freely flow into and out of the vacuum ball valve, increasing the convective and conductive losses the same way as for Configuration E. Second, the brass fitting at the bottom of the experimental Dewar was replaced with a Teflon one of the same dimensions. Compared to the worst performing Dewar, configuration E, the only difference between them was the material of the 1–1/2 in fitting at the bottom. The combination of this information confirms that replacing the high thermal conductivity brass fitting with a lower conductivity material improves performance of top and bottom dual opening Dewar design by reducing conductive losses to the outer Dewar shell. The evaporation curve for configuration D (Figure 3) is also revealing. Compared to configurations B, C, E, and F, the slope of the curve levels out faster as the volume of LN2 decreases. This is likely caused by an increasing amount of conductive surface area in contact with the LN2 being Teflon as the LN2 level lowers, versus being the stainless-steel or brass that is present in the other modified experimental Dewar configurations. It

is assumed that if configuration D was manufactured to hold a vacuum, such as configuration F, then the combination of a Teflon fitting and a vacuum jacket would prove to have better performance than configuration F.

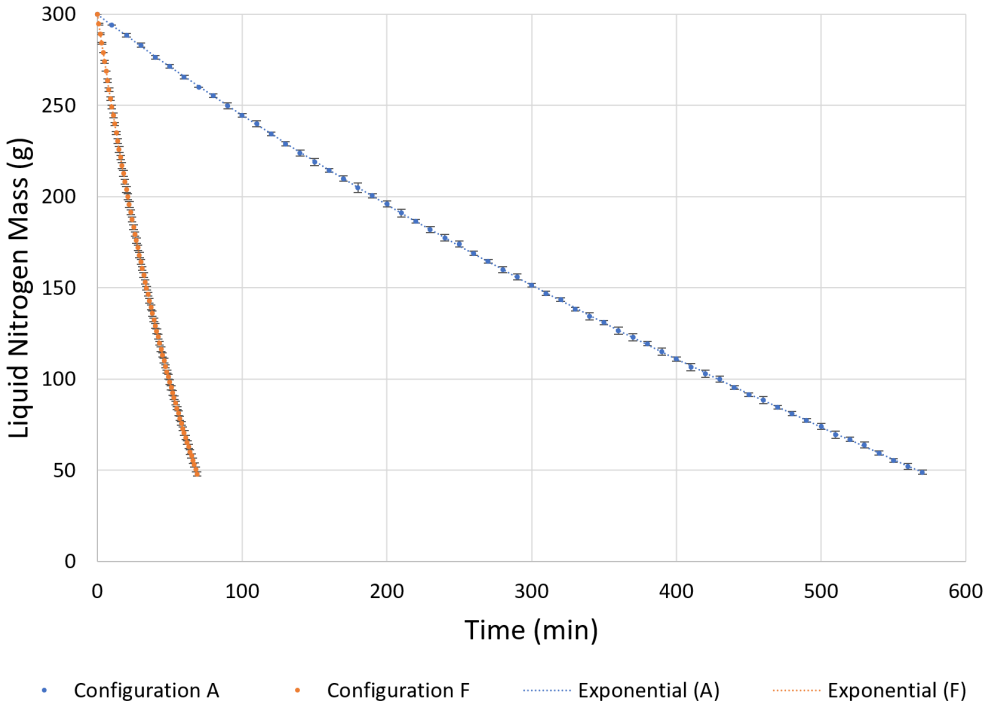

Evaporation rate of the baseline Dewar, configuration A, had the best performance and configuration F had the highest performance of modified experimental Dewars. Each curve is the average of four data runs, with data plotted in ten-minute increments for configuration A and one-minute increments for configuration F. Each data point contains y-axis LN2 mass error bars. Both curves start at 300 g of LN2 and continue until the first averaged data point is less than or equal to 50 g of LN2.

Figure 4. Evaporation Rates for Dewar Configurations A and F

Configuration C had the third best performance, with LN2 evaporating from 300 g to 49.5 g in 56 minutes. This configuration removed metal-to-metal conduction between the brass fitting and stainless-steel outer Dewar shell by removing a stainless-steel ring around the brass fitting. Though this configuration sacrifices being able to restore a vacuum to the Dewar, it still had better performance than Dewar configuration E; thus, it is confirmed that the metal-to-metal conduction at the brass fitting interface is

greater than the conduction of the brass-air-stainless steel interface produced. Despite this finding, it is still more advantageous to restore a vacuum jacket to the Dewar.

Experimental Dewar configuration B had the second worst performance, evaporating 250.5 g of LN2 in 48 minutes. This configuration merely removed the vacuum from between the inner and outer Dewar shells and did not add any brass fittings. Dewar configuration E had a similarly sized hole via the vacuum ball valve and barbed hose fitting, but also had the brass fitting protrude from the outer Dewar shell. The lack of this protrusion for configuration B likely accounts for its slightly better performance than configuration E.

Normalized exponential decay evaporation curve fit equations for each of the experimental Dewar Configurations were found using Equation 1.

$$y = (a)e^{-ba} + (c)e^{-dx} \tag{1}$$

where y is the normalized mass of LN2, x is the normalized elapsed experimental evaporation time, and a, b, c, and d are coefficients. Normalization was based on a 300 g LN2 initial mass and the associated evaporation time for a given experimental Dewar configuration. Table 2 contains the normalized evaporation equations and their associated R^2 value, as well as the final LN2 mass and evaporation time for each experimental Dewar configuration.

Table 2. Experimental Dewar Evaporation Equations

Experimental Dewar Configuration	Normalized Evaporation Equation and R^2 Value	Final LN2 Mass (g)	Evaporation Time (min)
A	$y=1.147e^{-0.8685x}-0.1477e^{0.7679x}$ $R^2=1.0000$	49.0	570
B	$y=1.081e^{-1.121x}-0.08338e^{0.811x}$ $R^2=1.0000$	49.5	48
C	$y=1.102e^{-1.07x}-0.1056e^{0.7096x}$ $R^2=1.0000$	49.5	56
D	$y=1.045e^{-1.317x}-0.04467e^{0.967x}$ $R^2=1.0000$	48.5	65
E	$y=1.207e^{-0.9559x}-0.2102e^{0.3818x}$ $R^2=1.0000$	46.5	46
F	$y=1.231e^{-0.9628x}-0.2302e^{0.2965x}$ $R^2=1.0000$	48.0	69

Experimental Dewar LN2 normalized evaporation equations, R^2 values, final mass, and evaporation times. Initial LN2 mass for all configurations was 300 g with a start time of zero minutes. Evaporation equations are valid when both x and y values are positive.

E. DISCUSSION

The LN2 storage performance of experimental Dewar configuration F is only 12.1% that of the baseline Dewar, configuration A. Despite the vacuum jacket greatly minimizing conduction through the vacuum space between the inner and outer Dewar shells, the increase in conduction between the bottom fittings and the outer Dewar shell, as well as the air and insulating foam around the producing fitting, greatly reduces the efficacy of LN2 storage, making the configuration F inappropriate for a system designed to produce LA in the container for later use on a small-scale remote, islanded, renewable microgrid. This is because these microgrids typically require the use of their stored within a day after production, such as during the night for solar based microgrids. Despite this, configuration F could be useful as a LA receiving vessel for a Stirling generator connected to the bottom port. This is because the energy lost at the bottom port is primarily conductive in nature and could be converted into electrical energy through an attached Stirling generator, with further energy recovery improvements possible by combining the Stirling generator with low temperature optimized thermoelectric generators (TEGs) on the outer Dewar shell.

These findings show that the dual opening Dewar design is insufficient for efficacious storage of LA for a directly connected cryocooler and energy recovery cycle. An alternative design is next proposed for development as future work. The proposed future design uses a COTS storage Dewar with a cryocooler connected to the top of the Dewar's neck. An elongated displacer chamber, or equivalent, would extend the cold finger of the cryocooler below the bottom of the neck and into the main storage volume of the Dewar, allowing for effective production of LA. It is proposed that the cryocooler make a pressure-tight connection with the Dewar upper opening except for two ports for connected tubing. One of these ports requires connection to a short tube to act as an air vent of the Dewar, allow for air to enter the Dewar for liquification during cryocooler operation and to prevent overpressure during normal LA storage. This vent would have a normally open electrical solenoid valve attached to it such that when the valve is energized and shuts the upper portion of the Dewar can be pressurized. Normal evaporation of LA in the Dewar would naturally increase its pressure. As pressure increases it forces the LA to travel through a low thermal conductivity tube, such as Teflon, that travels from the bottom of the LA storage volume and passes through the second port at the Dewar neck to a power recovery phase. This tube would act as a smaller, secondary neck of the Dewar, meaning it would slightly increase conductive losses via the neck opening, though this is likely minimal. Once a sufficient volume of LA has been delivered to the power recovery component, the solenoid valve would deenergize, reliving the internal pressure of the Dewar and allowing the LA to continue long-term, efficient storage. Figure 5 outlines a physical configuration for this proposed system.

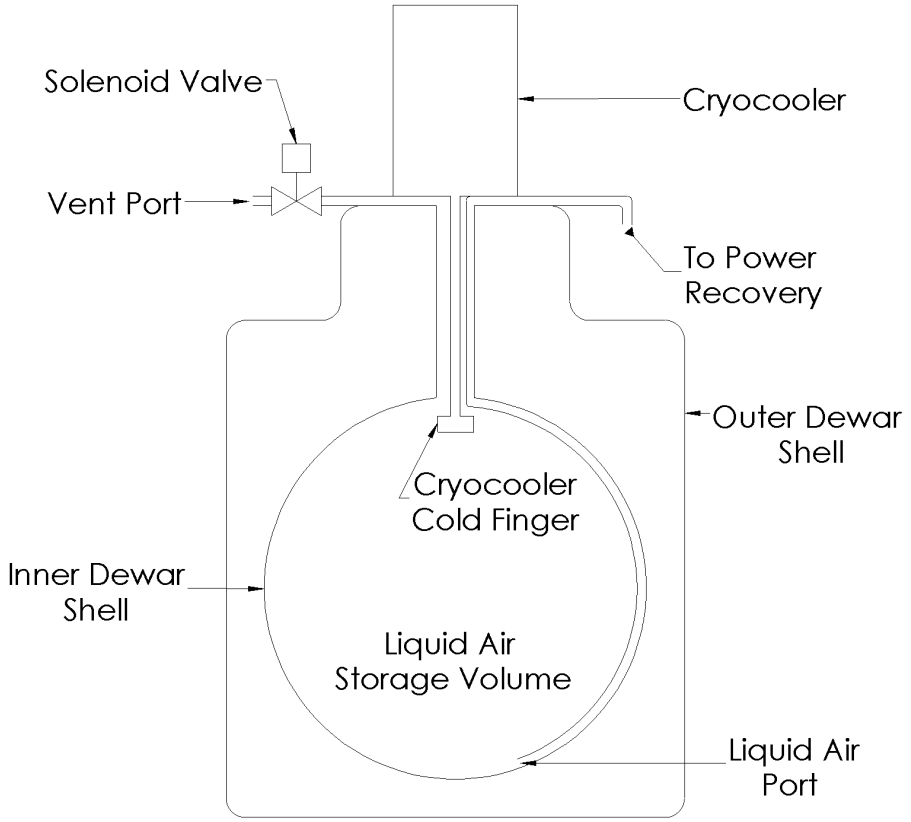

Dewar is normally unpressurized, but when power recovery is required by a connected microgrid, a solenoid valve on the vent port closes, allowing for a natural pressure increase to occur, forcing stored LA to be transported to a power recovery cycle.

Figure 5. Proposed LA Storage Dewar

This proposed LA storage Dewar configuration takes advantage of modern, optimized unpressurized Dewar design elements, which will allow for longer LA storage times while also leveraging natural evaporative processes to allow for the resultant pressure increase to transport LA from storage to a power recovery cycle. This design does add a small, periodic electrical load via the solenoid valve. Since a cryocooler must be operating with any configuration integrating a LA production system, a control system must be in place. This control system would likely be able to integrate control logic for the solenoid valve with minimal effort. It is recommended that a LA storage system following this design is built and tested for use on a small-scale, remote, islanded, and renewable microgrid.

F. CONCLUSIONS

A dual opening LA storage Dewar is not effective for storage times required for a small-scale remote, islanded, renewable microgrid; however, this dual opening Dewar design would be effective for shorter-term holding of LA while an energy recovery process, such as a Stirling generator, takes advantage of the thermal losses at the bottom opening. For a normally unpressurized LA storage system, it is recommended that a COTS Dewar is used in conjunction with a low-pressure, self-pressurizing LA transport system that can move LA from a high efficiency LA storage medium to a separate power recovery subsystem that is not in continuous contact with the stored LA medium.

G. PATENTS

Insights gained from the experimental Dewar configurations presented in Figure 3 resulted in the submission of U.S. Patent Application 63/343,020, 2022, titled "Two Opening Dewar with Desiccant Annulus." This Dewar is designed to be the receiving vessel for LA being used in conjunction with a Stirling generator. The Dewar design leverages a vacuum jacket to reduce convective and conductive thermal losses; Teflon inner Dewar walls to reduce conduction; dual layer reflective shielding to minimize radiative losses; Teflon to metal interfacing at the bottom Dewar penetration to reduce conductive energy losses from the Stirling generator metal fitting to the outer Dewar wall; and has an integrated desiccant annulus to minimize long-term moisture and accumulation within the Dewar.

THIS PAGE INTENTIONALLY LEFT BLANK

III. EXPERIMENTAL TEFLON DEWAR

This chapter outlines the novel Dewar created during the conduct of this thesis and the supporting information submitted in U.S. Patent Application 63/343,020, 2022, titled "Two Opening Dewar with Desiccant Annulus." Figure 6 illustrates this patented Dewar design using a coaxial, two-opening Dewar for implementation in a low-pressure, small-scale, Stirling-Stirling liquid air energy battery. A free-piston Stirling cryocooler liquefies air that has been dried with an integrated annular desiccant ring. The liquefied air falls through the Dewar vapor space and pools at the bottom of the vessel. The thermal cylinder head of a free piston Stirling generator passes through the bottom of the vessel and interfaces with a high thermal conductivity bushing and plug that conducts thermal energy from the pooled liquid to the generator.

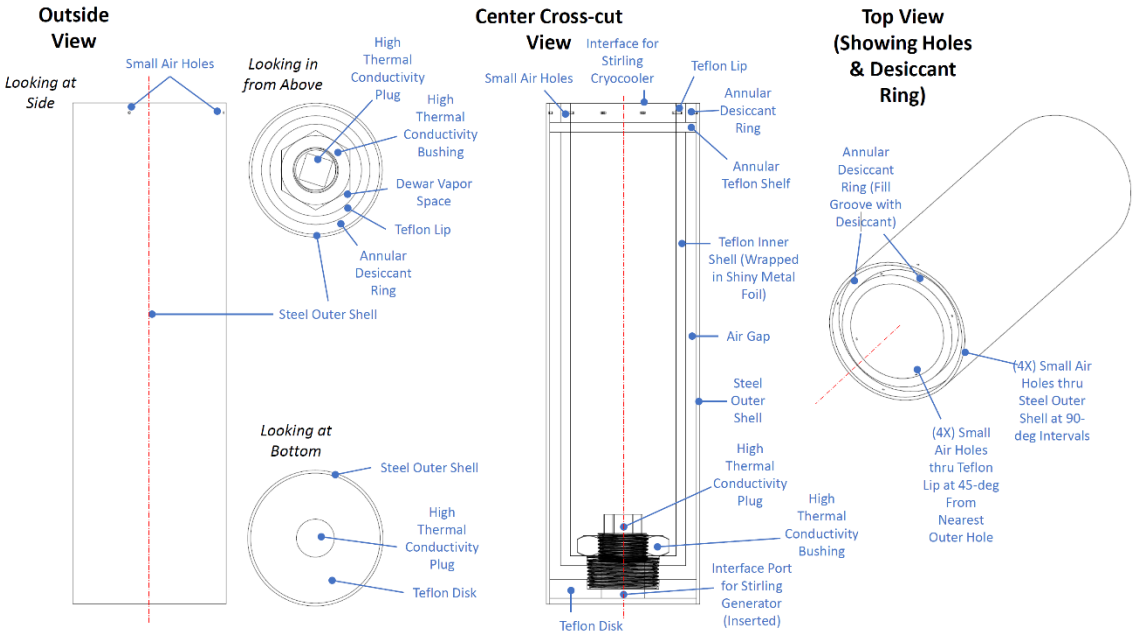

Figure 6. General Construction of Novel Teflon and Stainless-Steel Dewar with Stirling Generator Interface and Annular Desiccant Ring

The inner Dewar shell is made of Teflon. The top of the inner chamber is machined to have a Teflon lip and Teflon shelf, which creates a grove when mated with the Steel outer shell. This grove is filled with desiccant pellets, thus implementing an integrated annular desiccant ring. Four holes at 90-deg intervals are present at the top of the steel outer shell. Off-set by 45-deg, four holes are also present at the top of the Teflon inner shell above the Teflon shelf. Thus, dry air is ingested into the device to replace the air that has been liquefied by the Stirling Cryocooler. Teflon has favorable properties for cryogenic temperatures. Namely, Teflon, as a thermal insulator, will reduce conductive heat transfer radially, as well as from the inner to the outer vessel via the Dewar neck, which is a primary source of thermal losses in a traditional Dewar. The lower portion of the Teflon inner chamber is treaded and a plugged bushing (both made of high thermal conductive material) passes through the Dewar air, or vacuum, gap. This assembly serve as an interface for a Stirling generator. A counter-sunk, threaded Teflon disk interfaces with the bottom of the bushing in such a way as to create an air gap at the bottom of the Dewar. The steel outer shell slides over the Teflon disk at the bottom and over the annular Teflon shelf at the top. These serve as the only contact points for the steel outer shell.

The Teflon inner shell is wrapped in shiny, reflective foil to reduce radiative heat transfer. This layer is surround by a stagnant air gap, or vacuum (preferred), to reduce convective heat transfer. The air gap is created using a separation between the steel outer shell and the foil covered inner shell.

This design has several novel features with links to the intended function:

(1) The Dewar has two, coaxial openings of different sizes to allow for interfacing with a Stirling cryocooler and Stirling generator.

(2) A Teflon inner chamber reduces conductive heat transfer.

(3) The Dewar is fitted with an integrated, annular desiccant ring for drying low-pressure, ambient air.

The physical construction of this novel Teflon and Stainless-Steal Dewar, with integrated desiccant ring, is shown in Figure 7. The final working volume of this Dewar is 1150 ml.

(**a**) (**b**)

(b) Inner Dewar shell with dual reflective shielding (silver and gold foil), desiccant shelf, a hollow aluminum threaded fitting for interfacing to a Stirling generator, and a bottom Teflon disk to for a stagnant air or vacuum chamber; (**b**) Assembled Teflon and Stainless-Steel Dewar with a Stainless-Steel outer Dewar shell and a vacuum port for drawing a vacuum between the inner and outer Dewar shells.

Figure 7. Novel Teflon and Stainless-Steel Dewar

The only change to the physical construction of this Dewar and that shown in Figure 6 is that a vacuum valve was installed to establish a vacuum jacket; however, the Scotch-Weld Epoxy Adhesive 2216 B/A Gray proved to be ineffective at adequately bonding to Teflon to support drawing a vacuum, as was also seen in experimental Dewar Configuration D using a Teflon threaded fitting. Thus, a vacuum was not established, and

only stagnant air was achieved within the air gap between the inner and outer Dewar shells.

The same experimental setup and execution outlined in Chapter II.C was used to determine evaporation rates of this novel Dewar, which is designated as Configuration X. The only difference was that no 3D printed polylactic acid (PLA) plastic cylinder base was used due to the base of the Stainless-Steel cylinder exceeding this size (outside diameter of 4.5 in); additionally, the Stainless-Steel outer shell acted as its own support due to the design of the Stirling generator interface being recessed one inch from the bottom of the Stainless-Steel cylinder. Evaporation data for Configuration X is provided in Figure 8.

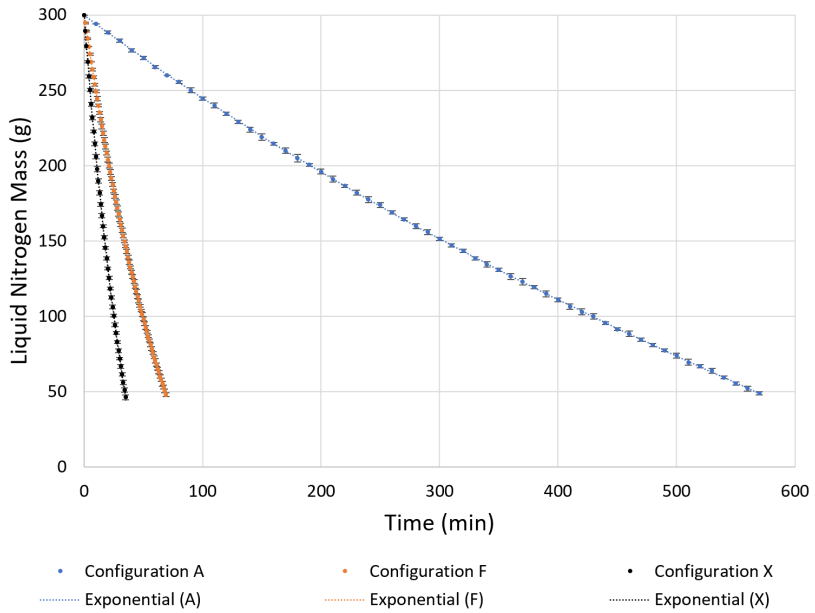

Evaporation rate of Configuration X performed worse than the best performing modified Experimental Dewar, Configuration F. Each curve is the average of four data runs, with data plotted in ten-minute increments for configuration A and one-minute increments for configuration F. Each data point contains y-axis LN2 mass error bars. Both curves start at 300 g of LN2 and continue until the first averaged data point is less than or equal to 50 g of LN2.

Figure 8. Evaporation Rates for Dewar Configurations A, F, and X

The evaporation rate of Configuration X was almost twice that of the best performing modified experimental Dewar, Configuration F. This is due to being unable to

establish a vacuum jacket for Configuration X, as well as the additional mass of Configuration X. The physical architectures between the configurations were also significantly different, with Configuration X having an internal volume of 150ml versus the Hydro Flask based experimental configurations which had a baseline volume of 473 ml; therefore, the results are not directly relatable, which is why the results for Configuration X were not included within the body of this Thesis. Normalization of Configuration X's evaporation rate data was also conducted using the same methodology outlined in Chapter II.D. The results of this process are shown in Table 3, along with the experimental Dewar configurations A and F.

Table 3. Evaporation Equations for Dewar Configurations A, F, and X

Experimental Dewar Configuration	Normalized Evaporation Equation and R^2 Value	Final LN2 Mass (g)	Evaporation Time (min)
A	$y=1.147e^{-0.8685x}-0.1477e^{0.7679x}$ $R^2=1.0000$	49.0	570
F	$y=1.231e^{-0.9628x}-0.2302e^{0.2965x}$ $R^2=1.0000$	48.0	69
X	$y=1.168e^{-0.9819x}-0.1682e^{0.5228x}$ $R^2=1.0000$	46.3	35

Experimental Dewar LN2 normalized evaporation equations, R^2 values, final mass, and evaporation times. Initial LN2 mass for all configurations was 300 g with a start time of zero minutes. Evaporation equations are valid when both x and y values are positive.

THIS PAGE INTENTIONALLY LEFT BLANK

IV. EXPERIMENTAL SETUP AND DATA

This chapter presents the physical experimental setup used for all data collection of this work, as well as the collected experimental data.

A. EXPERIMENTAL SETUP EXAMPLE

An example experimental setup, as described in Chapter II.C is shown in Figure 9.

Configuration E is shown on a 3D printed black polylactic acid (PLA) plastic cylinder base with a polyurethan ether foam cylinder on top of the Dewar. The Bonvoisin BCS-30 scale is also shown.

Figure 9. Example Experimental Setup

B. RAW EXPERIMENTAL DATA

Tables 4 through Table 10 show raw mass data for four data runs conducted on each experimental configuration, as well as average mass and standard deviation (SD).

Table 4. Configuration A Experimental Mass Data

Configuration A						
Time (min)	Run 1 Mass (g)	Run 2 Mass (g)	Run 3 Mass (g)	Run 4 Mass (g)	Average Mass (g)	SD (g)
0	300	300	300	300	300.0	0.0
10	294	294	294	294	294.0	0.0
20	290	288	288	288	288.5	1.0
30	282	282	284	284	283.0	1.2
40	276	276	278	276	276.5	1.0
50	270	272	272	272	271.5	1.0
60	264	266	266	266	265.5	1.0
70	260	260	260	260	260.0	0.0
80	254	256	256	256	255.5	1.0
90	248	250	250	252	250.0	1.6
100	244	244	244	246	244.5	1.0
110	238	240	240	242	240.0	1.6
120	234	234	234	236	234.5	1.0
130	228	228	230	230	229.0	1.2
140	222	224	224	226	224.0	1.6
150	218	218	218	222	219.0	2.0
160	214	214	214	216	214.5	1.0
170	208	210	210	212	210.0	1.6
180	202	206	204	208	205.0	2.6
190	200	200	200	202	200.5	1.0
200	194	196	196	198	196.0	1.6
210	190	190	190	194	191.0	2.0
220	186	186	186	188	186.5	1.0
230	180	182	182	184	182.0	1.6
240	176	178	176	180	177.5	1.9
250	172	174	174	176	174.0	1.6
260	168	170	168	170	169.0	1.2
270	164	164	164	166	164.5	1.0
280	158	160	160	162	160.0	1.6
290	154	156	156	158	156.0	1.6
300	150	152	152	152	151.5	1.0
310	146	148	146	148	147.0	1.2
320	142	144	144	144	143.5	1.0
330	138	138	138	140	138.5	1.0
340	132	136	134	136	134.5	1.9
350	130	130	132	132	131.0	1.2
360	124	128	126	128	126.5	1.9
370	120	124	124	124	123.0	2.0
380	118	120	120	120	119.5	1.0
390	112	116	116	116	115.0	2.0
400	110	110	112	112	111.0	1.2
410	104	108	106	108	106.5	1.9
420	100	104	104	104	103.0	2.0
430	98	100	100	102	100.0	1.6
440	94	96	96	96	95.5	1.0
450	90	92	92	92	91.5	1.0
460	86	88	90	90	88.5	1.9
470	84	84	84	86	84.5	1.0
480	80	80	82	82	81.0	1.2

Configuration A						
Time (min)	Run 1 Mass (g)	Run 2 Mass (g)	Run 3 Mass (g)	Run 4 Mass (g)	Average Mass (g)	SD (g)
490	76	78	78	78	77.5	1.0
500	72	74	74	76	74.0	1.6
510	68	68	70	72	69.5	1.9
520	66	66	68	68	67.0	1.2
530	62	64	64	66	64.0	1.6
540	58	60	60	60	59.5	1.0
550	54	56	56	56	55.5	1.0
560	50	52	52	54	52.0	1.6
570	48	50	48	50	49.0	1.2

Table 5. Configuration B Experimental Mass Data

Configuration B						
Time (min)	Run 1 Mass (g)	Run 2 Mass (g)	Run 3 Mass (g)	Run 4 Mass (g)	Average Mass (g)	SD (g)
0	300	300	300	300	300.0	0.0
1	290	292	292	292	291.5	1.0
2	284	284	284	284	284.0	0.0
3	276	276	274	278	276.0	1.6
4	268	268	266	270	268.0	1.6
5	262	260	260	262	261.0	1.2
6	256	254	252	254	254.0	1.6
7	248	246	244	248	246.5	1.9
8	240	240	238	240	239.5	1.0
9	236	234	232	236	234.5	1.9
10	228	226	224	228	226.5	1.9
11	222	220	220	222	221.0	1.2
12	216	214	214	216	215.0	1.2
13	210	208	208	210	209.0	1.2
14	204	202	202	204	203.0	1.2
15	198	196	194	198	196.5	1.9
16	192	190	188	192	190.5	1.9
17	186	184	182	188	185.0	2.6
18	180	178	178	182	179.5	1.9
19	174	172	172	176	173.5	1.9
20	168	166	166	170	167.5	1.9
21	164	162	162	166	163.5	1.9
22	158	156	158	160	158.0	1.6
23	152	150	152	154	152.0	1.6
24	148	146	146	148	147.0	1.2
25	144	142	142	144	143.0	1.2
26	138	136	138	140	138.0	1.6
27	132	132	132	134	132.5	1.0
28	128	128	128	130	128.5	1.0
29	124	124	124	126	124.5	1.0
30	118	118	120	122	119.5	1.9
31	114	114	116	118	115.5	1.9
32	110	110	112	112	111.0	1.2
33	106	106	108	108	107.0	1.2
34	102	100	102	104	102.0	1.6
35	96	98	98	98	97.5	1.0
36	92	94	94	96	94.0	1.6
37	88	90	90	90	89.5	1.0
38	84	86	88	86	86.0	1.6
39	80	82	82	84	82.0	1.6
40	76	78	80	80	78.5	1.9
41	72	76	76	76	75.0	2.0
42	68	72	72	72	71.0	2.0
43	64	68	68	68	67.0	2.0

Configuration B						
Time (min)	Run 1 Mass (g)	Run 2 Mass (g)	Run 3 Mass (g)	Run 4 Mass (g)	Average Mass (g)	SD (g)
44	60	64	64	64	63.0	2.0
45	58	60	60	62	60.0	1.6
46	54	56	56	58	56.0	1.6
47	50	54	54	56	53.5	2.5
48	46	50	50	52	49.5	2.5

Table 6. Configuration C Experimental Mass Data

Configuration C						
Time (min)	Run 1 Mass (g)	Run 2 Mass (g)	Run 3 Mass (g)	Run 4 Mass (g)	Average Mass (g)	SD (g)
0	300	300	300	300	300.0	0.0
1	294	294	294	292	293.5	1.0
2	286	288	286	284	286.0	1.6
3	280	282	280	276	279.5	2.5
4	274	274	272	268	272.0	2.8
5	266	270	266	262	266.0	3.3
6	260	262	260	256	259.5	2.5
7	254	256	256	250	254.0	2.8
8	248	250	250	246	248.5	1.9
9	242	244	244	240	242.5	1.9
10	236	240	238	234	237.0	2.6
11	232	234	232	228	231.5	2.5
12	226	228	226	224	226.0	1.6
13	220	222	222	218	220.5	1.9
14	214	216	216	214	215.0	1.2
15	208	210	212	208	209.5	1.9
16	204	206	206	204	205.0	1.2
17	198	200	202	200	200.0	1.6
18	194	194	196	196	195.0	1.2
19	188	190	190	190	189.5	1.0
20	184	184	186	186	185.0	1.2
21	180	180	180	180	180.0	0.0
22	174	174	176	176	175.0	1.2
23	170	170	174	172	171.5	1.9
24	166	164	168	168	166.5	1.9
25	160	160	164	164	162.0	2.3
26	156	156	158	160	157.5	1.9
27	152	150	154	156	153.0	2.6
28	148	148	148	152	149.0	2.0
29	144	142	146	146	144.5	1.9
30	138	138	142	142	140.0	2.3
31	134	134	138	138	136.0	2.3
32	132	130	132	134	132.0	1.6
33	126	126	130	130	128.0	2.3
34	122	122	126	126	124.0	2.3
35	118	118	122	122	120.0	2.3
36	116	114	118	118	116.5	1.9
37	112	110	114	114	112.5	1.9
38	106	106	110	110	108.0	2.3
39	104	102	106	108	105.0	2.6
40	100	100	102	104	101.5	1.9
41	96	96	98	100	97.5	1.9
42	92	92	96	96	94.0	2.3
43	90	88	92	94	91.0	2.6
44	86	84	90	88	87.0	2.6
45	82	82	84	86	83.5	1.9

Configuration C						
Time (min)	Run 1 Mass (g)	Run 2 Mass (g)	Run 3 Mass (g)	Run 4 Mass (g)	Average Mass (g)	SD (g)
46	78	78	82	82	80.0	2.3
47	76	74	78	80	77.0	2.6
48	72	72	74	76	73.5	1.9
49	70	68	70	72	70.0	1.6
50	66	66	68	70	67.5	1.9
51	62	62	66	66	64.0	2.3
52	60	60	62	64	61.5	1.9
53	56	56	60	60	58.0	2.3
54	54	54	56	58	55.5	1.9
55	50	52	54	54	52.5	1.9
56	48	48	50	52	49.5	1.9

Table 7. Configuration D Experimental Mass Data

Configuration D						
Time (min)	Run 1 Mass (g)	Run 2 Mass (g)	Run 3 Mass (g)	Run 4 Mass (g)	Average Mass (g)	SD (g)
0	300	300	300	300	300.0	0.0
1	292	292	294	294	293.0	1.2
2	286	286	288	286	286.5	1.0
3	282	280	280	280	280.5	1.0
4	276	274	276	274	275.0	1.2
5	270	268	268	268	268.5	1.0
6	264	262	264	262	263.0	1.2
7	258	258	258	256	257.5	1.0
8	252	252	252	250	251.5	1.0
9	246	246	246	244	245.5	1.0
10	240	242	240	240	240.5	1.0
11	234	236	236	234	235.0	1.2
12	230	232	230	228	230.0	1.6
13	226	226	226	224	225.5	1.0
14	220	220	220	218	219.5	1.0
15	214	216	216	214	215.0	1.2
16	210	210	210	208	209.5	1.0
17	206	206	206	204	205.5	1.0
18	200	200	200	200	200.0	0.0
19	196	196	196	194	195.5	1.0
20	192	192	192	190	191.5	1.0
21	186	186	186	186	186.0	0.0
22	182	184	182	182	182.5	1.0
23	178	178	178	176	177.5	1.0
24	172	174	176	172	173.5	1.9
25	168	170	170	168	169.0	1.2
26	164	166	166	164	165.0	1.2
27	160	162	162	160	161.0	1.2
28	156	158	158	156	157.0	1.2
29	152	154	154	152	153.0	1.2
30	148	150	150	148	149.0	1.2
31	144	146	146	144	145.0	1.2
32	142	142	142	140	141.5	1.0
33	138	140	140	138	139.0	1.2
34	134	136	136	134	135.0	1.2
35	130	132	132	130	131.0	1.2
36	128	128	128	126	127.5	1.0
37	124	126	126	124	125.0	1.2
38	122	122	124	120	122.0	1.6
39	118	120	120	116	118.5	1.9
40	114	116	116	114	115.0	1.2
41	112	114	112	110	112.0	1.6
42	108	110	110	108	109.0	1.2
43	106	106	106	104	105.5	1.0
44	102	104	104	102	103.0	1.2
45	100	100	100	98	99.5	1.0

Configuration D						
Time (min)	Run 1 Mass (g)	Run 2 Mass (g)	Run 3 Mass (g)	Run 4 Mass (g)	Average Mass (g)	SD (g)
46	98	98	98	96	97.5	1.0
47	94	94	94	92	93.5	1.0
48	90	92	92	90	91.0	1.2
49	88	90	90	88	89.0	1.2
50	86	86	86	84	85.5	1.0
51	82	84	84	82	83.0	1.2
52	80	80	82	80	80.5	1.0
53	78	78	78	76	77.5	1.0
54	74	76	76	74	75.0	1.2
55	72	74	74	72	73.0	1.2
56	70	72	72	68	70.5	1.9
57	66	68	70	66	67.5	1.9
58	64	66	66	62	64.5	1.9
59	64	64	64	60	63.0	2.0
60	60	60	62	58	60.0	1.6
61	58	58	58	56	57.5	1.0
62	56	56	56	54	55.5	1.0
63	52	54	54	52	53.0	1.2
64	50	52	52	48	50.5	1.9
65	48	50	48	48	48.5	1.0

Table 8. Configuration E Experimental Mass Data

Configuration E						
Time (min)	Run 1 Mass (g)	Run 2 Mass (g)	Run 3 Mass (g)	Run 4 Mass (g)	Average Mass (g)	SD (g)
0	300	300	300	300	300.0	0.0
1	292	290	292	292	291.5	1.0
2	284	282	284	284	283.5	1.0
3	276	274	276	274	275.0	1.2
4	270	266	270	266	268.0	2.3
5	262	258	262	260	260.5	1.9
6	254	252	254	252	253.0	1.2
7	248	244	248	246	246.5	1.9
8	240	238	240	238	239.0	1.2
9	234	230	234	232	232.5	1.9
10	228	224	226	224	225.5	1.9
11	220	218	220	218	219.0	1.2
12	214	210	214	212	212.5	1.9
13	208	206	208	206	207.0	1.2
14	200	200	200	200	200.0	0.0
15	194	192	194	194	193.5	1.0
16	188	186	188	188	187.5	1.0
17	184	180	184	182	182.5	1.9
18	178	174	178	176	176.5	1.9
19	170	168	172	170	170.0	1.6
20	166	164	166	166	165.5	1.0
21	160	158	160	160	159.5	1.0
22	154	152	156	154	154.0	1.6
23	150	146	150	150	149.0	2.0
24	144	140	144	144	143.0	2.0
25	138	134	138	138	137.0	2.0
26	134	130	134	134	133.0	2.0
27	128	124	128	128	127.0	2.0
28	124	120	124	124	123.0	2.0
29	118	116	120	118	118.0	1.6
30	114	110	114	114	113.0	2.0
31	108	106	112	110	109.0	2.6
32	104	100	106	106	104.0	2.8
33	100	96	100	100	99.0	2.0

Configuration E						
Time (min)	Run 1 Mass (g)	Run 2 Mass (g)	Run 3 Mass (g)	Run 4 Mass (g)	Average Mass (g)	SD (g)
34	96	92	96	96	95.0	2.0
35	92	88	92	92	91.0	2.0
36	86	84	86	88	86.0	1.6
37	82	80	82	84	82.0	1.6
38	78	76	78	80	78.0	1.6
39	74	72	74	76	74.0	1.6
40	72	68	70	72	70.5	1.9
41	66	64	66	68	66.0	1.6
42	62	60	62	64	62.0	1.6
43	58	56	58	60	58.0	1.6
44	54	52	54	56	54.0	1.6
45	52	50	50	54	51.5	1.9
46	46	46	46	48	46.5	1.0

Table 9. Configuration F Experimental Mass Data

Configuration F						
Time (min)	Run 1 Mass (g)	Run 2 Mass (g)	Run 3 Mass (g)	Run 4 Mass (g)	Average Mass (g)	SD (g)
0	300	300	300	300	300.0	0.0
1	295	294	295	295	294.8	0.5
2	289	289	289	290	289.3	0.5
3	285	284	284	284	284.3	0.5
4	279	279	279	279	279.0	0.0
5	274	275	273	274	274.0	0.8
6	269	269	269	269	269.0	0.0
7	264	265	263	263	263.8	1.0
8	259	260	258	258	258.8	1.0
9	254	255	253	253	253.8	1.0
10	250	250	249	248	249.3	1.0
11	245	246	244	243	244.5	1.3
12	240	241	240	239	240.0	0.8
13	235	236	235	234	235.0	0.8
14	231	232	230	229	230.5	1.3
15	226	228	226	224	226.0	1.6
16	222	223	221	220	221.5	1.3
17	217	219	217	215	217.0	1.6
18	212	215	213	211	212.8	1.7
19	208	210	208	207	208.3	1.3
20	204	206	204	202	204.0	1.6
21	200	202	200	198	200.0	1.6
22	195	198	196	194	195.8	1.7
23	191	193	192	190	191.5	1.3
24	187	189	188	186	187.5	1.3
25	183	185	183	182	183.3	1.3
26	179	181	180	178	179.5	1.3
27	175	178	176	175	176.0	1.4
28	171	174	172	171	172.0	1.4
29	167	170	168	167	168.0	1.4
30	163	166	164	164	164.3	1.3
31	160	162	161	160	160.8	1.0
32	156	159	157	156	157.0	1.4
33	152	155	153	153	153.3	1.3
34	149	151	150	149	149.8	1.0
35	146	148	146	146	146.5	1.0
36	142	145	143	142	143.0	1.4
37	138	141	139	139	139.3	1.3
38	135	138	136	135	136.0	1.4
39	132	134	132	132	132.5	1.0
40	128	131	129	129	129.3	1.3
41	125	128	126	126	126.3	1.3
42	122	125	123	123	123.3	1.3
43	119	121	120	119	119.8	1.0
44	115	118	117	116	116.5	1.3
45	112	115	113	113	113.3	1.3
46	109	112	110	110	110.3	1.3
47	106	108	107	107	107.0	0.8

Configuration F						
Time (min)	Run 1 Mass (g)	Run 2 Mass (g)	Run 3 Mass (g)	Run 4 Mass (g)	Average Mass (g)	SD (g)
48	103	105	104	104	104.0	0.8
49	100	103	101	101	101.3	1.3
50	97	100	98	98	98.3	1.3
51	94	97	95	95	95.3	1.3
52	91	94	92	93	92.5	1.3
53	89	91	89	90	89.8	1.0
54	86	88	86	87	86.8	1.0
55	83	85	84	84	84.0	0.8
56	80	83	81	81	81.3	1.3
57	77	80	78	79	78.5	1.3
58	75	77	75	76	75.8	1.0
59	72	74	72	73	72.8	1.0
60	69	72	70	71	70.5	1.3
61	67	69	67	69	68.0	1.2
62	65	66	64	66	65.3	1.0
63	62	64	62	64	63.0	1.2
64	59	61	59	61	60.0	1.2
65	57	59	57	59	58.0	1.2
66	54	56	54	57	55.3	1.5
67	52	54	52	54	53.0	1.2
68	50	51	49	52	50.5	1.3
69	47	49	47	49	48.0	1.2

Table 10. Configuration X Mass Data

Configuration X						
Time (min)	Run 1 Mass (g)	Run 2 Mass (g)	Run 3 Mass (g)	Run 4 Mass (g)	Average Mass (g)	SD (g)
0	300	300	300	300	300.0	0.0
1	289	289	290	290	289.5	0.6
2	279	278	280	280	279.3	1.0
3	269	268	269	270	269.0	0.8
4	259	258	260	260	259.3	1.0
5	250	249	251	251	250.3	1.0
6	241	239	241	242	240.8	1.3
7	232	230	232	233	231.8	1.3
8	222	222	223	224	222.8	1.0
9	214	213	215	216	214.5	1.3
10	205	205	206	208	206.0	1.4
11	197	196	198	200	197.8	1.7
12	189	189	190	192	190.0	1.4
13	181	181	182	184	182.0	1.4
14	174	173	174	176	174.3	1.3
15	166	166	167	169	167.0	1.4
16	159	159	160	161	159.8	1.0
17	152	152	152	154	152.5	1.0
18	145	145	145	147	145.5	1.0
19	138	138	138	140	138.5	1.0
20	132	131	131	133	131.8	1.0
21	125	125	125	127	125.5	1.0
22	118	118	118	120	118.5	1.0
23	112	112	112	114	112.5	1.0
24	106	106	105	108	106.3	1.3
25	100	100	100	102	100.5	1.0
26	94	94	93	96	94.3	1.3
27	89	89	88	90	89.0	0.8
28	83	83	82	84	83.0	0.8
29	77	77	76	79	77.3	1.3
30	72	72	71	73	72.0	0.8
31	67	67	65	68	66.8	1.3
32	62	62	60	62	61.5	1.0
33	56	57	54	57	56.0	1.4

Configuration X						
Time (min)	Run 1 Mass (g)	Run 2 Mass (g)	Run 3 Mass (g)	Run 4 Mass (g)	Average Mass (g)	SD (g)
34	52	51	49	52	51.0	1.4
35	47	47	44	47	46.3	1.5

THIS PAGE INTENTIONALLY LEFT BLANK

V. CONCLUSION

A. CONCLUSIONS

This thesis showed that a dual opening LA storage Dewar is not effective for the short-term (i.e., 24 hours) storage times required for a small-scale remote, islanded, renewable military microgrid to effectively utilize the stored energy of LA. This is due to excessive conductive thermal losses at the bottom opening, which physically bridges the outer and inner Dewar shells. This thermal bridge causes stored energy to rapidly be lost as heat is transmitted from the outer Dewar shell to the inner Dewar shell. While not effective for short-term LA storage, this design could be effective for receiving LA from a different LA storage vessel for immediate use with an energy recovery process, such as a Stirling or thermoelectric generator, that can advantage of the thermal losses at the bottom opening.

Configuration F, coupled with the baseline Configuration A, emphasized the importance of a vacuum jacket for a Dewar vice stagnant air, providing strong evidence that any Dewar should have this feature. Additionally, Configuration D showed that the use of Teflon does improve storage time and that this configuration would likely exceed the storage effectiveness of the best performing experimental Dewar, Configuration F, if a vacuum was effectively maintained. This is due to the more desirable (i.e., low) thermal conductivity of Teflon.

B. FUTURE WORK

Though this work determined that a dual opening Dewar is likely not effective for use on a small-scale microgrid, further scaling analysis could be conducted using greater storage volumes with similar evaporation rates, allowing the volume of stored LA to be maintained up to 24 hours. Further analysis could also be conducted using different cryocooler options. This would allow for a LA production versus LA evaporation analysis to be conducted, determining the amount of excess energy, and time, a microgrid would require to effectively use this dual opening Dewar as a storage medium. Additionally, this type of Dewar could be used to implement a personal cooling system,

like the U.S. Army's Light-Weight Environmental Control System (LWECS), which circulates refrigerant to minimize heat related injuries to personnel [48].

Further investigation into the production of a Teflon based Dewar is also recommended. If a vacuum-tight Teflon-metal interface is achieved, initial evidence of this work shows that a Dewar leveraging Teflon's low thermal conductivity material should prove more efficacious at storing cryogenic liquid, at least for short-term storage where conductive heat transfer is the primary means of thermal losses. Machining both the inner and outer Dewar shells from a single, continuous piece of Teflon would also help to minimize interfaces that would require establishing a vacuum seal.

While further investigation of using this dual opening Dewar could be conducted as a coupling between LA production and power recovery, the design is better suited for receiving LA and storing it for immediate use while it is being used to recover electrical power. Thus, for a normally unpressurized LA storage system, it is recommended that a COTS Dewar is used in conjunction with a low-pressure, self-pressurizing LA transport system that can move LA from a high efficiency LA storage medium to a separate power recovery subsystem that is not in continuous contact with the stored LA medium. This removes the thermal bridge between the inner and outer Dewar shells, which caused excessive conductive losses for the analyzed experimental Dewars. This design, as presented in Chapter II.E, is recommended to be built and tested as future work. An alternative to extending the cryocooler displacer chamber of the proposed self-pressurizing design is to extend its cold finger. Swanson et. al. presented work showing the advantages of a cold finger extension [36]. Further analysis could prove that this method, which is likely easier and more cost effective to implement than elongating the cryocooler displacer chamber, though this would need to be verified in future work.

The self-pressurizing Dewar design has the potential to improve on several existing and proposed small-scale microgrid systems. One such system, presented by Varley et. al., proposes the development of a shipping container-enclosed microgrid using Lithium-ion batteries [49]. Replacing these batteries with a small-scale LAES system could reduce the size of the needed battery bank, allowing for additional storage room for

portable photovoltaic cells and reducing the weight of the shipping container as it is moved between desired sites.

Finally, future work should analyze the resilience and cost tradespace for implementing this type of LAES system on a small-scale microgrid. Giachetti et. al. have conducted this work for microgrids with multiple power sources, to include renewables and diesel generators, and battery storage options [50]. This would provide useful insights into the economic and operational effectiveness of pursuing this type of LAES system further.

THIS PAGE INTENTIONALLY LEFT BLANK

LIST OF REFERENCES

[1] S. Padmanaban, K. Nithiyananthan, S. P. Karthikeyan, and J. B. Holm-Nielsen, *Microgrids*, 1st ed. Boca Raton, Florida: CRC Press, 2020 [Online]. Available: https://doi.org/10.1201/9780367815929.

[2] R. Haerer, "Whack-a-mole fuel selection: Reducing operational risks and mitigating new challenges in the U.S. Department of Defense." Climate and Security Fellowship Program, Oct. 2021. [Online]. Available: https://climateandsecurity.org/wp-content/uploads/2021/10/Climate-Security-Risk-Briefers_Climate-and-Security-Fellows-Program_October-2021-1.pdf#page=27

[3] S. Van Broekhoven, N. Judson, J. Galvin, and J. Marqusee, "Leading the charge: Microgrids for domestic military installations," *IEEE Power Energy Mag.*, vol. 11, no. 4, pp. 40–45, Jul. 2013 [Online]. Available: doi: 10.1109/MPE.2013.2258280.

[4] A. Mercurio, "Microgrids and energy security: The business case," in International Association for Energy Economics, pp. 45–47, 2013 [Online]. Available: http://www.iaee.org/documents/2013EnergyForum4qtr.pdf.

[5] J. M. Raya-Armenta, N. Bazmohammadi, J. G. Avina-Cervantes, D. Sáez, J. C. Vasquez, and J. M. Guerrero, "Energy management system optimization in islanded microgrids: An overview and future trends," *Renew. Sustain. Energy Rev.*, vol. 149, p. 111327, Oct. 2021 [Online]. Available: https://doi.org/10.1016/j.rser.2021.111327.

[6] D. T. Ton and M. A. Smith, "The U.S. Department of Energy's microgrid initiative," *Electr. J.*, vol. 25, no. 8, pp. 84–94, Oct. 2012 [Online]. Available: https://doi.org/10.1016/j.tej.2012.09.013.

[7] G. P. Holdmann, R. W. Wies, and J. B. Vandermeer, "Renewable energy integration in Alaska's remote islanded microgrids: Economic drivers, technical strategies, technological niche development, and policy implications," *Proc. IEEE*, vol. 107, no. 9, pp. 1820–1837, Sep. 2019 [Online]. Available: https://doi.org/10.1109/JPROC.2019.2932755.

[8] A. Hirsch, Y. Parag, and J. Guerrero, "Microgrids: A review of technologies, key drivers, and outstanding issues," *Renew. Sustain. Energy Rev.*, vol. 90, pp. 402–411, Jul. 2018 [Online]. Available: https://doi.org/10.1016/j.rser.2018.03.040.

[9] E. Anuat, D. L. Van Bossuyt, and A. Pollman, "Energy resilience impact of supply chain network disruption to military microgrids," *Infrastructures*, vol. 7, no. 1, Art. no. 1, Jan. 2022 [Online]. Available: https://doi.org/10.3390/infrastructures7010004.

[10] R. E. Giachetti, C. J. Peterson, D. L. Van Bossuyt, and G. W. Parker, "Systems engineering issues in microgrids for military installations," *INCOSE Int. Symp.*, vol. 30, no. 1, pp. 731–746, Jul. 2020 [Online]. Available: https://doi.org/10.1002/j.2334-5837.2020.00751.x.

[11] B. S. Blanchard and W. J. Fabrycky, *Systems engineering and analysis*, 5th ed. Boston: Prentice Hall, 2011.

[12] C. J. Peterson, D. L. Van Bossuyt, R. E. Giachetti, and G. Oriti, "Analyzing mission impact of military installations microgrid for resilience," *Systems*, vol. 9, no. 3, Art. no. 3, Sep. 2021 [Online]. Available: https://doi.org/10.3390/systems9030069.

[13] E. Wood, "Microgrid defined: Three key features that make a microgrid a microgrid," *Microgrid Knowledge*, Mar. 28, 2020. https://microgridknowledge.com/microgrid-defined/ (accessed Aug. 02, 2022).

[14] D. Ton and J. Reilly, "Microgrid controller initiatives: An overview of R&D by the U.S. Department of Energy," *IEEE Power Energy Mag.*, vol. 15, no. 4, pp. 24–31, Jul. 2017 [Online]. Available: https://doi.org/10.1109/MPE.2017.2691238.

[15] T. Caldognetto, P. Tenti, A. Costabeber, and P. Mattavelli, "Improving microgrid performance by cooperative control of distributed energy sources," *IEEE Trans. Ind. Appl.*, vol. 50, no. 6, pp. 3921–3930, Nov. 2014 [Online]. Available: https://doi.org/10.1109/TIA.2014.2313648.

[16] C. Schwaegerl, L. Tao, P. Mancarella, and G. Strbac, "Can microgrids provide a new paradigm for network operation? An evaluation of their technical, commercial and environmental benefits," in *CIRED 2009 – 20th International Conference and Exhibition on Electricity Distribution – Part 1*, Jun. 2009, pp. 1–4.

[17] Department of the Navy, "NAVFAC P-602 3-Pillars of Energy Security (Reliability, Resilience, & Efficiency)." Washington Navy Yard, DC, 2021. [Online]. Available: https://www.wbdg.org/FFC/NAVFAC/PPUBB/P-602_rev2.pdf

[18] A. Kafetzis, C. Ziogou, K. D. Panopoulos, S. Papadopoulou, P. Seferlis, and S. Voutetakis, "Energy management strategies based on hybrid automata for islanded microgrids with renewable sources, batteries and hydrogen," *Renew. Sustain. Energy Rev.*, vol. 134, p. 110118, Dec. 2020 [Online]. Available: https://doi.org/10.1016/j.rser.2020.110118.

[19] S. Ganesan, U. Subramaniam, A. A. Ghodke, R. M. Elavarasan, K. Raju, and M. S. Bhaskar, "Investigation on sizing of voltage source for a battery energy storage system in microgrid with renewable energy sources," *IEEE Access*, vol. 8, pp. 188861–188874, 2020 [Online]. Available: https://doi.org/10.1109/ACCESS.2020.3030729.

[20] J. Liu, H. Chen, W. Zhang, B. Yurkovich, and G. Rizzoni, "Energy management problems under uncertainties for grid-connected microgrids: A chance constrained programming approach," *IEEE Trans. Smart Grid*, vol. 8, no. 6, pp. 2585–2596, Nov. 2017 [Online]. Available: https://doi.org/10.1109/TSG.2016.2531004.

[21] M. S. Ismail, M. Moghavvemi, T. M. I. Mahlia, K. M. Muttaqi, and S. Moghavvemi, "Effective utilization of excess energy in standalone hybrid renewable energy systems for improving comfort ability and reducing cost of energy: A review and analysis," *Renew. Sustain. Energy Rev.*, vol. 42, pp. 726–734, Feb. 2015 [Online]. Available: https://doi.org/10.1016/j.rser.2014.10.051.

[22] M. Altin, A. D. Hansen, T. K. Barlas, K. Das, and J. N. Sakamuri, "Optimization of short-term overproduction response of variable speed wind turbines," *IEEE Trans. Sustain. Energy*, vol. 9, no. 4, pp. 1732–1739, Oct. 2018 [Online]. Available: https://doi.org/10.1109/TSTE.2018.2810898.

[23] M. M. Rahman, A. O. Oni, E. Gemechu, and A. Kumar, "Assessment of energy storage technologies: A review," *Energy Convers. Manag.*, vol. 223, p. 113295, Nov. 2020 [Online]. Available: https://doi.org/10.1016/j.enconman.2020.113295.

[24] S. Koohi-Fayegh and M. A. Rosen, "A review of energy storage types, applications and recent developments," *J. Energy Storage*, vol. 27, p. 101047, Feb. 2020 [Online]. Available: https://doi.org/10.1016/j.est.2019.101047.

[25] V. Musolino, A. Pievatolo, and E. Tironi, "A statistical approach to electrical storage sizing with application to the recovery of braking energy," *Energy*, vol. 36, no. 11, pp. 6697–6704, Nov. 2011 [Online]. Available: https://doi.org/10.1016/j.energy.2011.07.037.

[26] O. O'Callaghan and P. Donnellan, "Liquid air energy storage systems: A review," *Renew. Sustain. Energy Rev.*, vol. 146, p. 111113, Aug. 2021 [Online]. Available: https://doi.org/10.1016/j.rser.2021.111113.

[27] C. Damak, D. Leducq, H. M. Hoang, D. Negro, and A. Delahaye, "Liquid air energy storage (LAES) as a large-scale storage technology for renewable energy integration – A review of investigation studies and near perspectives of LAES," *Int. J. Refrig.*, vol. 110, pp. 208–218, Feb. 2020 [Online]. Available: https://doi.org/10.1016/j.ijrefrig.2019.11.009.

[28] E. Borri, A. Tafone, A. Romagnoli, and G. Comodi, "A review on liquid air energy storage: History, state of the art and recent developments," *Renew. Sustain. Energy Rev.*, vol. 137, p. 110572, Mar. 2021 [Online]. Available: https://doi.org/10.1016/j.rser.2020.110572.

[29] S. X. Wang, X. D. Xue, X. L. Zhang, J. Guo, Y. Zhou, and J. J. Wang, "The application of cryogens in liquid fluid energy storage systems," *Phys. Procedia*, vol. 67, pp. 728–732, Jan. 2015 [Online]. Available: https://doi.org/10.1016/j.phpro.2015.06.123.

[30] A. Benato and A. Stoppato, "Pumped thermal electricity storage: A technology overview," *Therm. Sci. Eng. Prog.*, vol. 6, pp. 301–315, Jun. 2018 [Online]. Available: https://doi.org/10.1016/j.tsep.2018.01.017.

[31] D. M. Joshi and H. K. Patel, "Analysis of cryogenic cycle with process modeling tool: Aspen HYSYS," *J. Instrum.*, vol. 10, no. 10, pp. T10001–T10001, Oct. 2015 [Online]. Available: https://doi.org/10.1088/1748-0221/10/10/T10001.

[32] T. A. Howe, A. G. Pollman, and A. J. Gannon, "Operating range for a combined, building-scale liquid air energy storage and expansion system: Energy and exergy analysis," *Entropy*, vol. 20, no. 10, Art. no. 10, Oct. 2018 [Online]. Available: https://doi.org/10.3390/e20100770.

[33] R. Willis, A. Pollman, A. Gannon, and A. Hernandez, "Preliminary modeling of a building-scale liquid air energy storage systems using Aspen HYSYS," Monterey, CA., Jun. 2018.

[34] C. Girouard, A. Pollman, and A. Hernandez, "Modeling and simulation informed conceptual design, analysis, and initial component selection of a supply-side building scale laes system for renewable, islanded microgrid resiliency," Colorado Springs, CO, Jun. 2019.

[35] A. Fredrickson, A. Pollman, A. Gannon, and W. Smith, "Selection of a heat exchanger for a small-scale liquid air energy storage system," Anaheim, CA, Jul. 2021 [Online]. Available: https://doi.org/10.1115/POWER2021-60523.

[36] H. M. Swanson, A. G. Pollman, and A. Hernandez, "Experimental evaluation of dewar volume and cryocooler cold finger size in a small-scale stirling liquid air energy storage (LAES) system," presented at the ASME 2021 Power Conference, Aug. 2021 [Online]. Available: https://doi.org/10.1115/POWER2021-60565.

[37] M. Torosyan, A. Pollman, A. Gannon, and A. Hernandez, "Performance and complexity trade study of candidate liquid air generation techniques," presented at the ASME 2021 Power Conference, Aug. 2021 [Online]. Available: https://doi.org/10.1115/POWER2021-63957.

[38] N. A. Bailey, C. M. Girouard, and A. G. Pollman, "Dual stirling cycle liquid air battery," US20220042478A1, Feb. 10, 2022. Accessed: Aug. 03, 2022. [Online]. Available: https://patents.google.com/patent/US20220042478A1/en

[39] S. Arnold, C. Fackrell, D. Horton, A. Pollman, F. Smeeks, and J. Sweet, "Need, function, and requirements analysis for liquid air energy storage prototype on a military microgrid," Quantico, VA, Jun. 01, 2022 [Online]. Available: https://doi.org/10.13140/RG.2.2.31342.28481.

[40] Y. Lobunets, "Thermoelectric generator for utilizing cold energy of cryogen liquids," *J. Electron. Mater.*, vol. 48, no. 9, pp. 5491–5496, Sep. 2019 [Online]. Available: https://doi.org/10.1007/s11664-019-07392-3.

[41] R. Barron and G. Nellis, *Cryogenic Heat Transfer*, Second. CRC Press, 2016.

[42] T. D. Bostock and R. G. Scurlock, *Low-Loss Storage and Handling of Cryogenic Liquids: The Application of Cryogenic Fluid Dynamics*. Cham, Switzerland: Springer International Publishing, 2019.

[43] P. Lynam, A. Mustafa, W. Proctor, and R. Scurlock, "Reduction of the heat flux into liquid helium in wide necked metal dewars," *Cryogenics*, vol. 9, no. 4, pp. 242–247, Aug. 1969 [Online]. Available: https://doi.org/10.1016/0011-2275(69)90229-X.

[44] E. T. Swartz, "Efficient cryogenic design, a system approach," *J. Low Temp. Phys.*, vol. 101, no. 1–2, pp. 249–252, Oct. 1995 [Online]. Available: https://doi.org/10.1007/BF00754584.

[45] B. O'Halloran, "System Engineering Theses: A Manuscript Option." Jul. 31, 2017. [Online]. Available: https://libguides.nps.edu/ld.php?content_id=34397759

[46] N. A. Bailey, A. G. Pollman, and E. P. Paulo, "Energy recovery for dual-Stirling liquid air energy storage prototype," presented at the ASME 2020 Power Conference collocated with the 2020 International Conference on Nuclear Engineering, Oct. 2020 [Online]. Available: https://doi.org/10.1115/POWER2020-16087.

[47] "National institute of standards and technology," *NIST*. https://www.nist.gov/ (accessed Aug. 16, 2022).

[48] E. Palermo, "US troops beat the heat with new personal AC units," *livescience.com*, Aug. 13, 2014. https://www.livescience.com/47327-army-personal-cooling-systems.html (accessed Oct. 31, 2022).

[49] D. Varley, D. Van Bossuyt, and A. Pollman, "Feasibility Analysis of a Mobile Microgrid Design to Support DOD Energy Resilience Goals," Systems, vol. 10, p. 74, Jun. 2022 [Online]. Available: https://doi.org/10.3390/systems10030074.

[50] R. Giachetti, D. Van Bossuyt, W. Anderson, and G. Oriti, “Resilience and Cost Trade Space for Microgrids on Islands,” IEEE Systems Journal, vol. PP, pp. 1–11, Aug. 2021 [Online]. Available: https://doi.org/10.1109/JSYST.2021.3103831.

INITIAL DISTRIBUTION LIST

1. Defense Technical Information Center
   Ft. Belvoir, Virginia

2. Dudley Knox Library
   Naval Postgraduate School
   Monterey, California